1-1-2006

A quasi-two-dimensional finite element formulation for analysis of active-passive constrained layer beams

Jean-Jacques R. Boiluea Bekuit
Ryerson University

A QUASI-TWO-DIMENSIONAL FINITE ELEMENT FORMULATION FOR ANALYSIS OF ACTIVE-PASSIVE CONSTRAINED LAYER BEAMS

BY

JEAN-JACQUES R. BOILEAU BEKUIT
M. SC. (AEROSPACE) KIEV UNIVERSITY OF CA
UKRAINE, 1997

A THESIS

PRESENTED TO RYERSON UNIVERSITY

IN PARTIAL FULFILLMENT OF THE
REQUIREMENTS FOR THE DEGREE OF
MASTER OF APPLIED SCIENCE
IN THE DEPARTEMENT OF
MECHANICAL ENGINEERING

TORONTO, ONTARIO, CANADA, 2006

I hereby declare that I am the sole author of this thesis.

I authorize Ryerson University to lend this thesis to other institutions or individuals for the purpose of scholarly research.

Signature_

I furhter authorize Ryerson Uinversity to reproduce this thesis by photocpying or by other means, in total or in part, at the request of other institutions or individuals for the purpose of scholarly research.

Signature_

Abstract

A QUASI-TWO-DIMENSIONAL FINITE ELEMENT FORMULATION FOR ANALYSIS OF ACTIVE-PASSIVE CONSTRAINED LAYER BEAMS

Jean-Jacques R. Boileau Bekuit
Master of Applied Science
Graduate Program in Mechanical Engineering
Ryerson University
2006

Active-passive damping is getting more popular with designers because it combines the complementary passive and active features in the control of structural vibrations. The classical three-layer structure has a viscoelastic-layer sandwiched between the host beam and a piezoelectric-layer.

The more prevalent assumptions for modeling the system are the use of Euler-Bernoulli beam theory for both the host beam and piezoelectric-layer, and Timoshenko beam theory for the viscoelastic-layer. The assumption that transverse displacement is constant through the thickness limits accuracy and applicability of the model. The current formulation expresses the through-the-thickness dependency of the field variables as polynomials while their span dependency across a finite element is cubically interpolated.

The versatility of the formulation is demonstrated via static and dynamic studies of examples taken from the literature. A beam treated with active-passive damping is presented and examined. The constitutive relation of the viscoelastic layer is represented using fractional derivatives and the Grünwald approximation. The extended Hamilton's principle is used to derive the system governing equations which are integrated with the Newmark time-integration scheme.

Acknowledgement

I would like to express my sincere gratitude to my supervisor Dr. Donatus Oguamanam for his guidance throughout my studies and this project.

I am also grateful to Jocelyne Boileau Bekuit, my wife, for her proofreading assistance despite the fact that most of the material is strange to her. Patience during the preparation of this manuscript was a great motivation. I am particularly thankful to my colleague Asif Shariff for his help with MATLAB programming.

Last but not least, I am thankful to my daughter Anaïs Bekuit for her understanding; instead of spending valuable time with her I was locked in my office working on this manuscript.

DEDICATION

I couldn't have done this without the help of my family and friends.

Table of Contents

AUTHOR'S DECLARATION. ii

ABSTRACT. iii

ACKNOWLEDGEMENT. iv

DEDICATION. v

TABLE OF CONTENTS. vi

LIST OF TABLES. viii

LIST OF FIGURES. ix

NOMENCLATURE. x

CHAPTER 1 INTRODUCTION. 1

CHAPTER 2 MATHEMATICAL FORMULATIONS. 4

2.1 System Description. 4

2.2 Kinematic Assumptions. 5

2.2.1 Bottom Layer. 5

2.2.2 Core. 6

2.2.3 Top Layer. 8

2.3 Constitutive Equations. 10

2.3.1 Bottom Layer. 10

2.3.2 Core. 11

2.3.3 Top Layer. 13

2.4 Variational Formulation. 15

2.4.1 Bottom Layer. 15

2.4.2 Core. 16

2.4.3 Top Layer. 19

CHAPTER 3 FINITE ELEMENT MODELING. 21
3.1 Mapping. 22
3.1.1 Bottom Layer. 22
3.1.2 Core. 23
3.1.3 Top Layer. 24
3.2 Shape Functions. 25
3.2.1 Bottom Layer. 25
3.2.2 Core. 26
3.2.3 Top Layer. 28
3.3 Equation of Motion. 29
CHAPTER 4 NUMERICAL SIMULATION. 31
4.1 Validation. 31
4.1.1 Piezo-Aluminium Sandwich Beam. 31
4.1.2 Sandwich Beam with Soft Core. 35
4.1.3 Visco-Aluminium Sandwich Beam. 36
4.2 Sample Simulation. 37
4.2.1 Case of Fully Constrained Layer Beam. 38
4.2.2 Case of Partially-Constrained-Layer Beam. 41
CHAPTER 5 CONCLUSION. 44
REFERENCES. 45

List of Tables

4.1 Mechanical Properties of piezo-aluminium sandwich beam. 32
4.2 Mechanical Properties of soft core-steel sandwich beam. 35
4.3 Comparison of first 10 natural frequencies. 36
4.4 Mechanical Properties of Visco-Aluminium sandwich beam. 37

List of Figures

2.1 Schematic of the composite beam 4

3.1 Schematic of a finite element 21

4.1 Piezo-Aluminium Sandwich beam 31

4.2 Transverse Displacement along the span of the beam 32

4.3 Through-the-thickness Axial Stress Distribution at mid-span of the beam 33

4.4 Through-the-thickness Axial Stress distribution in the core ($h_c = 16\,mm$). . . . 33

4.5 Through-the-thickness Axial Stress distribution in the core ($h_c = 10\,mm$). . . . 34

4.6 Through-the-thickness Axial Stress distribution in the core ($h_c = 4\,mm$). . . . 34

4.7 Deflection for Various values of core thickness (h_c) 34

4.8 Visco-Aluminium Sandwich beam and Load 36

4.9 Dynamic Response of The Viscoelastic Sandwich beam 37

4.10 Schematic of a fully constrained layer beam 38

4.11 Tip deflection and actuator voltage of a fully constrained layer beam subjected to a triangular impulse load at the free end. 39

4.12 Tip deflection and actuator voltage of a fully constrained layer beam subjected to a harmonic force ($0.1sin150t$) at the free end. 40

4.13 Schematic of a partially-constrained-layer beam 41

4.14 Tip deflection and actuator voltage of a partially-constrained-layer beam subjected to a triangular impulse load at the free end. 42

4.15 Tip deflection and actuator voltage of a partially-constrained-layer beam subjected to a harmonic force ($0.1sin150t$) at the free end. 43

Nomenclature

L	=	length of the beam	ϵ_i, γ_{ij}	=	strains
b	=	width of the beam	$\tilde{\varepsilon}_c$	=	core anelastic strain vector
h	=	total height of the beam	$\tilde{\varepsilon}_i$	=	strain vectors
h_i	=	thickness coordinates	σ_i, τ_{ij}	=	stresses
ρ_i	=	density	$\bar{\sigma}_c$	=	core anelastic stresses
ν_i	=	Poisson's ratio	V	=	voltage
x, z	=	beam coordinates	E_z	=	electrical field
t	=	temporal variable	D_z	=	electrical displ. field
Q_i	=	elastic matrices	τ	=	relaxation time
$\bar{Q}_i$	=	reduced elastic matrices	Δt	=	time step
C_i	=	compliance matrices	u	=	axial displacement
$\tilde{C}_c$	=	anelastic compliance matrices	w	=	transverse displacement
c_{ij}	=	elastic constants	$\tilde{u}_c$	=	anelastic displacement
e_{ij}	=	piezoelectric constants	q_e	=	elemental displ. vector
d_{ij}	=	dielectric permittivity	M, K	=	mass, stiffness matrices
D_i	=	operator matrix	N_i	=	shape functions
α	=	fractional derivative order	J	=	jacobian
$()_p$	=	piezo layer subscript	a_i, e_i, l_i	=	displ. fields coefficients
$()_c$	=	visco layer subscript	c_i, m_i, n_i		
$()_b$	=	beam layer subscript	δ	=	variation function
E_i	=	Young's modulus	T	=	kinetic energy
K_c	=	core elastic stiffness matrices	U	=	strain energy
$\tilde{K}_c$	=	core anelastic stiffness matrices	$\tilde{U}_c$	=	anelastic strain energy
$\hat{()}$	=	electric component	W	=	work
$\tilde{()}$	=	viscoelastic component	$\tilde{W}_c$	=	work of anelastic force
u_i	=	displacement vector	F	=	force matrix
$\bar{u}_i$	=	local displacement vector	ω	=	natural frequencies
I_i	=	mass and inertia moment	E_0	=	static elastic modulus
k	=	shear correction factor	E_∞	=	dynamic elastic modulus

Chapter 1

Introduction

The ever increasing demand for strong, stiff, lightweight materials for use in a wide range of structures has also increased the demand for engineers to address the repetitive motion and noise of mechanical systems, ranging from simple structures such as machine parts to the more complex such as spacecrafts.

Different techniques have been suggested for suppressing vibration and noise without compromising on stiffness, weight and complexity. An investigation of the different techniques and the progress made in recent years was compiled by Stanway and Rongong [1]. This involved structural design, localized additions of masses or neutralizers, isolation of a body from the excitation source and additions of damping by the means of a constrained layer to the host structure, which is the most widely used because it gives designers an option to control the vibrations of the structure.

Many researchers have devoted their work in recent years to constrained layer damping treatment as the means to control vibration in elastic structures. Among the modeling issues facing the designers are: the kinematics, the viscoelastic models and the control strategies. Constrained layer damping(CLD) can be divided into three categories: Passive (PCLD), Active (ACLD) and Active-Passive or Smart (SCLD).

Passive damping is achieved by adding a viscoelastic layer sandwich between the host structure and a constraining elastic layer. The constraining layer is passive because it is not contributing in the damping process; damping is achieved by the dissipative properties of the viscoelastic materials. This technique is widely used in practical applications because of its simplicity. It is very effective at high frequencies in reducing the amplitudes, structural fatigue

and noise. However, viscoelastic materials are very sensitive to temperature and frequencies. They are ineffective at low frequencies [1].

Active damping is generally achieved by attaching a piezoelectric layer to a host beam. The piezoelectric layer is called active because of its ability to respond to the desired degree of damping. Active damping is "smart" if the system is free of an external source. Peng and Lam [2] studied a system in which the host beam is sandwiched between distributed piezoelectric actuators and sensors. They employed a third-order displacement theory based finite element.

Active-Passive damping is a hybrid approach that integrates both passive and active damping. The constraining layer in passive damping is replaced by a piezoelectric-layer. The combination of passive and active damping gives both reliability and control over the vibrations of the structures. Yi and Ling [3] designed a three layer composite laminate. Prony series were used to model the viscoelastic material and a solid element was adopted for finite element modeling. Balamurugan and Narayanan [4] used a partially covered smart constrained layer. The viscoelastic layer was modeled using the Golla-Hughes-Mctavish (GHM) time domain approach [5, 6]. A C_0 finite element modeling was adopted and reduced integration was used to eliminate shear locking.

The analysis of a composite beam focuses on individual layer behavior. The assumptions of the classical three-layer models are ([7, 8, 9]): (1) negligible in-plane core stiffness with the core supporting only shear, (2) constant transverse displacement at any cross section, (3) perfect bonding between the layers, (4) thinness and infinite stiffness of the bonding adhesive layers, (5) adequacy of Euler-Bernoulli beam theory for the constraining layer and the host structure and Timoshenko beam theory for the viscoelastic layer, (6) dominance of inertia from transverse flexural motion, (7) smallness of deformations and strains, and (8) displacement variation is generally piece-wise linear with partial continuity. An investigation of the different formulations is reported in [10], which also examines an extension where transverse shear is included in the host beam and constrained layer as in Reference [4]. Most of these formulations ignore transverse shear and/or shear stress which can be significant in certain structures. Therefore, their application and accuracy are limited. Also, they require the use of different methods to address shear locking. The most accurate method for analyzing these structures is the use of a

three-dimensional brick finite element [3]. However, this results in complexity in the formulation and increases computational time because a huge number of elements is needed in order to avoid problems due to aspect ratio.

The higher order finite elements method proposed by Oskooei and Hansen [11] for static analysis of sandwich structures, and later extended to dynamic analysis by Nabarrete and De Almeida [12], is very instructive. A quasi-three-dimensional finite element formulation is obtained by assuming a polynomial expansion of all field variables through the thickness of the appropriate layer and interpolating their in-plane variance via the use of bicubic Lagrange shape functions. The core anti-plane behavior is not assumed. Hence, the in-plane properties of the viscoelastic-layer are explicitly included in the formulation.

The current study closely follows the concept presented in [11] and [12] to develop a quasi-two-dimensional finite element formulation for analysis of active-passive constrained layer beams. The composite structure is a Timoshenko beam for all layers. The deformations assumptions of the constraining layer and the host beam are derived from the theory of laminated beams [13]. For the core, the axial displacement is cubic in the thickness coordinates while the transverse displacement is quadratic in the thickness coordinates. This will prevent shear locking in the core.

The integration over the thickness is done a priori in closed-form in the variational formulation while a Gaussian quadrature [14] numerical integration is used over the span. Thus, a quasi-two-dimensional formulation is obtained.

To validate the current formulation, three examples from the existing literature are presented. Results are compared with the present formulation for both the static and dynamic analysis. The fidelity of the formulation in relation to sandwich beams with viscoelastic cores is also presented. A host beam with active-passive constrained layer damping is examined. Results are presented and analyzed. A sensor voltage feedback control is adopted.

Chapter 2

Mathematical Formulations

2.1 System Description

A schematic of the composite beam with a segment of the span covered with an active constrained layer is illustrated in Fig. 2.1. The composite beam comprises three layers and has a rectangular cross section. The bottom layer identified by the letter b is made of isotropic, linearly elastic material. The core c is a viscoelastic material and the top or constraining layer p is made of piezoelectric material. The latter has the ability to act both as a sensor and an actuator. Some of the configurations available to designers were compiled by Stanway and Rongong [1]. A sensor/actuator configuration is adopted in this work because of its simplicity. The composite beam is divided into two sections: *section* (1) is the beam segment that is treated with the active constrained layer and *section* (2) comprises only one elastic layer b

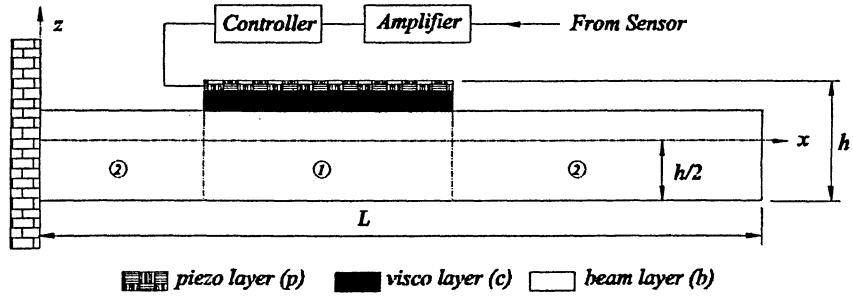

Figure 2.1: Schematic of the composite beam

The geometry of the composite beam is such that it has a length L, width b and heights h_i where $i \in \{p, c, b\}$; $h = \sum h_i$ is the total height of the composite beam and $z = \frac{h}{2}$ is taken as the reference surface. The material properties of each layer are density ρ_i, Young's modulus of elasticity E_i and Poisson's ratio ν_i. All layers are perfectly bonded; the adhesive layers are thin with infinite stiffness.

2.2 Kinematic Assumptions

2.2.1 Bottom Layer (Host Beam)

The axial and transverse displacement of the host beam are u and w, respectively. The displacement vector u_b is given as:

$$u_b = \begin{Bmatrix} u \\ w \end{Bmatrix} = \begin{Bmatrix} a_0 + z a_1 \\ l_0 \end{Bmatrix}$$

The coefficients a_0, a_1 and l_0 are functions of the spatial variable x and temporal variable t. This kinematic form is able to capture both Euler-Bernoulli and Timoshenko beam theories. The coordinate of any point in the thickness direction from the reference surface is represented by z. The reference surface is taken at the geometric midpoint of the composite beam. Defining a new vector $\{\bar{u}_b\}^T = \begin{Bmatrix} a_0 & a_1 & l_0 \end{Bmatrix}$, u_b can be expanded as:

$$u_b = \begin{bmatrix} 1 & z & 0 \\ 0 & 0 & 1 \end{bmatrix} \begin{Bmatrix} a_0 \\ a_1 \\ l_0 \end{Bmatrix} \equiv [Z_b] \{\bar{u}_b\} \tag{2.1}$$

The corresponding strain-displacement relation is linear and given by [15]:

$$\begin{cases} \epsilon_x = \dfrac{\partial u}{\partial x} = a_{0,x} + z a_{1,x} \\ \gamma_{zx} = \dfrac{\partial u}{\partial z} + \dfrac{\partial w}{\partial x} = a_1 + l_{0,x} \end{cases} \tag{2.2}$$

The strain vector ε_b takes the form $\varepsilon_b = \left\{ \begin{array}{c} \epsilon_x \\ \gamma_{zx} \end{array} \right\} = \left\{ \begin{array}{c} a_{0,x} + z a_{1,x} \\ a_1 + l_{0,x} \end{array} \right\}$ which can be reduced to the following compact expression:

$$\varepsilon_b = \begin{bmatrix} 1 & z & 0 & 0 \\ 0 & 0 & 1 & 1 \end{bmatrix} \left[D_b \right] \left\{ \begin{array}{c} a_0 \\ a_1 \\ l_0 \end{array} \right\} \equiv \left[\tilde{Z}_b \right] [D_b] \{\bar{u}_b\} \tag{2.3}$$

where the operator matrix $[D_b]$ is given as:

$$[D_b] = \begin{bmatrix} \frac{\partial}{\partial x} & 0 & 0 \\ 0 & \frac{\partial}{\partial x} & 0 \\ 0 & 1 & 0 \\ 0 & 0 & \frac{\partial}{\partial x} \end{bmatrix}$$

2.2.2 Core (Visco)

The axial displacement u is interpolated through the thickness by a cubic function while the transverse w displacement is quadratically interpolated. The displacement vector u_c takes the form:

$$u_c = \left\{ \begin{array}{c} u \\ w \end{array} \right\} = \left\{ \begin{array}{c} c_0 + z c_1 + z^2 c_2 + z^3 c_3 \\ m_0 + z m_1 + z^2 m_2 \end{array} \right\}$$

where the coefficients c_0, c_1, c_2, c_3, m_0, m_1 and m_2 are functions of the spatial variable x and temporal variable t. This relation is expanded by the use of a new vector $\{\bar{u}_c\}^T = \left\{ \begin{array}{ccccccc} c_0 & c_1 & c_2 & c_3 & m_0 & m_1 & m_2 \end{array} \right\}$ as:

$$u_c = \begin{bmatrix} 1 & z & z^2 & z^3 & 0 & 0 & 0 \\ 0 & 0 & 0 & 0 & 1 & z & z^2 \end{bmatrix} \begin{Bmatrix} c_0 \\ c_1 \\ c_2 \\ c_3 \\ m_0 \\ m_1 \\ m_2 \end{Bmatrix} \equiv [Z_c]\{\bar{u}_c\} \tag{2.4}$$

with the corresponding strain-displacement components [15] written as:

$$\begin{cases} \epsilon_x = \dfrac{\partial u}{\partial x} = c_{0,x} + zc_{1,x} + z^2c_{2,x} + z^3c_{3,x} \\ \epsilon_z = \dfrac{\partial w}{\partial z} = m_1 + 2zm_2 \\ \gamma_{xz} = \dfrac{\partial u}{\partial z} + \dfrac{\partial w}{\partial x} = c_1 + 2zc_2 + 3z^2c_3 + m_{0,x} + zm_{1,x} + z^2m_{2,x} \end{cases}$$

The strain vector ε_c takes the form $\varepsilon_c = \begin{Bmatrix} \epsilon_x \\ \epsilon_z \\ \gamma_{zx} \end{Bmatrix}$ and a compact matrix notation is given as:

$$\varepsilon_c = \begin{bmatrix} 1 & z & z^2 & z^3 & 0 & 0 & 0 & 0 & 0 & 0 & 0 & 0 \\ 0 & 0 & 0 & 0 & 1 & 2z & 0 & 0 & 0 & 0 & 0 & 0 \\ 0 & 0 & 0 & 0 & 0 & 0 & 1 & 2z & 3z^2 & 1 & z & z^2 \end{bmatrix} [D_c] \begin{Bmatrix} c_0 \\ c_1 \\ c_2 \\ c_3 \\ m_0 \\ m_1 \\ m_2 \end{Bmatrix} \equiv \left[\tilde{Z}_c\right] [D_c]\{\bar{u}_c\} \tag{2.5}$$

where the operator matrix $[D_c]$ is given as:

$$[D_c] = \begin{bmatrix} \frac{\partial}{\partial x} & 0 & 0 & 0 & 0 & 0 & 0 \\ 0 & \frac{\partial}{\partial x} & 0 & 0 & 0 & 0 & 0 \\ 0 & 0 & \frac{\partial}{\partial x} & 0 & 0 & 0 & 0 \\ 0 & 0 & 0 & \frac{\partial}{\partial x} & 0 & 0 & 0 \\ 0 & 0 & 0 & 0 & 0 & 1 & 0 \\ 0 & 0 & 0 & 0 & 0 & 0 & 1 \\ 0 & 1 & 0 & 0 & 0 & 0 & 0 \\ 0 & 0 & 1 & 0 & 0 & 0 & 0 \\ 0 & 0 & 0 & 1 & 0 & 0 & 0 \\ 0 & 0 & 0 & 0 & \frac{\partial}{\partial x} & 0 & 0 \\ 0 & 0 & 0 & 0 & 0 & \frac{\partial}{\partial x} & 0 \\ 0 & 0 & 0 & 0 & 0 & 0 & \frac{\partial}{\partial x} \end{bmatrix}$$

2.2.3 Top Layer (Piezo)

Mechanical

The formulation of the piezoelectric layer is similar to the formulation of the beam layer insofar as the mechanical aspect is concerned. Here, as in the preceding subsections, the coefficients e_0, e_1 and n_0 are functions of the spatial variable x and temporal variable t. The displacement vector u_p is given as:

$$u_p = \begin{Bmatrix} u \\ w \end{Bmatrix} = \begin{Bmatrix} e_0 + ze_1 \\ n_0 \end{Bmatrix}$$

Introducing a new vector $\{\bar{u}_p\}^T = \begin{Bmatrix} e_0 & e_1 & n_0 \end{Bmatrix}$, u_p is rewritten as:

$$u_p = \begin{bmatrix} 1 & z & 0 \\ 0 & 0 & 1 \end{bmatrix} \begin{Bmatrix} e_0 \\ e_1 \\ n_0 \end{Bmatrix} \equiv [Z_p] \{\bar{u}_p\} \tag{2.6}$$

The corresponding strain-displacement components [15] are given by:

$$\begin{cases} \epsilon_x = \dfrac{\partial u}{\partial x} = e_{0,x} + z e_{1,x} \\ \gamma_{zx} = \dfrac{\partial u}{\partial z} + \dfrac{\partial w}{\partial x} = e_1 + n_{0,x} \end{cases} \tag{2.7}$$

The strain vector ε_p takes the form $\varepsilon_p = \begin{Bmatrix} \epsilon_x \\ \gamma_{zx} \end{Bmatrix} = \begin{Bmatrix} e_{0,x} + z e_{1,x} \\ e_1 + n_{0,x} \end{Bmatrix}$, which in matrix form corresponds to:

$$\varepsilon_p = \begin{bmatrix} 1 & z & 0 & 0 \\ 0 & 0 & 1 & 1 \end{bmatrix} \begin{bmatrix} D_p \end{bmatrix} \begin{Bmatrix} e_0 \\ e_1 \\ n_0 \end{Bmatrix} \equiv \begin{bmatrix} \bar{Z}_p \end{bmatrix} \begin{bmatrix} D_p \end{bmatrix} \{\bar{u}_p\} \tag{2.8}$$

where the operator matrix $[D_p]$ is given as:

$$[D_p] = \begin{bmatrix} \dfrac{\partial}{\partial x} & 0 & 0 \\ 0 & \dfrac{\partial}{\partial x} & 0 \\ 0 & 1 & 0 \\ 0 & 0 & \dfrac{\partial}{\partial x} \end{bmatrix}$$

Electrical

The electrical potential ψ_p is assumed to be linear within the thickness of the piezoelectric layer and is given by [16]:

$$\psi_p = \psi_0(x,t) + z\psi_1(x,t) \tag{2.9}$$

where ψ_0 and ψ_1 represent the electric potential and its gradient at the midplane of the layer respectively. Neglecting the axial component of the electrical field (i.e., $E_x = 0$), one can obtain the expression of the transverse electrical field by differentiating Eq. (2.9) with respect to z:

$$E_z = \frac{\partial \psi_p}{\partial z} = \psi_1 \tag{2.10}$$

If $V(x,t)$ is the voltage applied to the piezoelectric layer, then $\psi_1 = -\frac{V(x,t)}{h_p}$. Therefore, the final expression of E_z can be written as:

$$E_z = -\frac{V(x,t)}{h_p} \tag{2.11}$$

where h_p is the thickness of the piezo layer.

2.3 Constitutive Equations

2.3.1 Bottom Layer (Host Beam)

The two dimensional (x, z plane) stress-strain constitutive relation for an isotropic material is given by [17]:

$$\begin{Bmatrix} \sigma_x \\ \sigma_z \\ \tau_{zx} \end{Bmatrix} = \begin{bmatrix} c_{11} & c_{13} & 0 \\ c_{13} & c_{33} & 0 \\ 0 & 0 & c_{66} \end{bmatrix} \begin{Bmatrix} \epsilon_x \\ \epsilon_z \\ \gamma_{zx} \end{Bmatrix} \tag{2.12}$$

where σ_x and σ_z, represent the stress in x and z direction respectively, τ_{zx} is the shear stress and c_{ij} are elastic constants of the material. Assuming that stress in the z direction is zero ($i.e.,\ \ \sigma_z = 0$), then $\epsilon_z = -\frac{c_{13}}{c_{33}}\,\epsilon_x$ and $\bar{c}_{11} = \left(c_{11} - \frac{c_{13}^2}{c_{33}}\right)$ which permits the use of the constitutive relation in the form:

$$\sigma_b = \begin{Bmatrix} \sigma_x \\ \tau_{zx} \end{Bmatrix} = \begin{bmatrix} \bar{c}_{11} & 0 \\ 0 & \bar{c}_{66} \end{bmatrix} \begin{Bmatrix} \epsilon_x \\ \gamma_{zx} \end{Bmatrix} \equiv \begin{bmatrix} \overline{Q}_b \end{bmatrix} \varepsilon_b \tag{2.13}$$

For an isotropic material, $\bar{c}_{11} = \dfrac{E_b}{1-\nu_b^2}$ and $\bar{c}_{66} = k\dfrac{\nu_b E_b}{2(1+\nu_b)}$ where k is the shear correction factor and E_b and ν_b represent the Young elastic modulus and the Poisson ratio respectively.

2.3.2 Core (Visco)

Elastic Properties

The core experiences both longitudinal and transverse stresses $\sigma_z \neq 0$; hence, the constitutive relation is identical to Eq. (2.12):

$$\bar{\sigma}_c = \begin{Bmatrix} \sigma_x \\ \sigma_z \\ \tau_{zx} \end{Bmatrix} = \begin{bmatrix} c_{11} & c_{13} & 0 \\ c_{13} & c_{33} & 0 \\ 0 & 0 & c_{66} \end{bmatrix} \begin{Bmatrix} \epsilon_x \\ \epsilon_z \\ \gamma_{zx} \end{Bmatrix} = [Q_c]\,\varepsilon_c \tag{2.14}$$

For an isotropic material, using plane strain assumptions, $c_{11} = c_{33} = \dfrac{(1-\nu_c)E_c}{(1-2\nu_c)(1+\nu_c)}$ $c_{13} = \dfrac{\nu_c E_c}{(1-2\nu_c)(1+\nu_c)}$ and $c_{66} = \dfrac{\nu_c E_c}{2(1+\nu_c)}$.

Viscoelastic Properties

Modeling of the viscoelastic layer presents many options to the designer. The choice is often dictated by the type of solution the designer wants to generate or by the control law. The simplest model is the complex modulus: $E^* = E' + iE''$ where E' and E'' are constants [3]. The Prony series model is also popular in commercial software because of low numerical cost. The other model is the Golla-Hughes-McTavish (GHM) [4, 8, 9]. This model allows time-domain simulation. The major shortcoming is the addition of extra degrees of freedom which increases computation cost. If the designer is interested in the dynamic properties of the viscoelastic layer, then the fractional derivative model (FD) is the most suitable [18].

Viscoelastic materials are time dependant; their mechanical behavior at any given time depends not only on the current state of stress and strain but also on the full history. This behavior can be mathematically modeled by a four-parameter fractional derivative model as [19]:

$$\bar{\sigma}_c(t) + \tau^\alpha \frac{d^\alpha \bar{\sigma}_c(t)}{dt^\alpha} = E_0[\zeta]\varepsilon_c(t) + \tau^\alpha E_\infty[\zeta]\frac{d^\alpha \varepsilon_c(t)}{dt^\alpha} \tag{2.15}$$

The above equation represents the constitutive relation of the viscoelastic core, where E_0 is the static elastic modulus (when the frequency $\omega \longrightarrow 0$), E_∞ denotes the dynamic elas-

tic modulus (when the frequency $\omega \longrightarrow \infty$), τ is the relaxation time and is strictly positive, α, which varies between 0 and 1, is the fractional derivative order, $\frac{d^\alpha}{dt^\alpha}$ is the fractional derivative operator and $[\zeta] = \begin{bmatrix} \zeta_{11} & \zeta_{13} & 0 \\ \zeta_{13} & \zeta_{33} & 0 \\ 0 & 0 & \zeta_{66} \end{bmatrix}$ with $\zeta_{11} = \zeta_{33} = \frac{(1-\nu_c)}{(1-2\nu_c)(1+\nu_c)}$, $\zeta_{13} = \frac{\nu_c}{(1-2\nu_c)(1+\nu_c)}$ and $\zeta_{66} = \frac{\nu_c}{2(1+\nu_c)}$.

The anelastic strain $\tilde{\varepsilon}_c(t)$ can be written as:

$$\tilde{\varepsilon}_c(t) = \varepsilon_c(t) - [\zeta]^{-1}\frac{\bar{\sigma}_c(t)}{E_\infty} \tag{2.16}$$

which permits Eq. (2.15) to be rewritten as:

$$\left(\frac{E_\infty - E_0}{E_\infty}\right)\varepsilon_c(t) = \tilde{\varepsilon}_c(t) + \tau^\alpha \frac{d^\alpha \tilde{\varepsilon}_c(t)}{dt^\alpha} \tag{2.17}$$

The advantage of this expression is that there is only one fractional derivative term.

Using the Grünwald definition to approximate the fractional derivative operator $\frac{d^\alpha}{dt^\alpha}$, Galucio et al. [19] show that at a given time t the anelastic strain can be expressed as:

$$\tilde{\varepsilon}_c(t) = (1-\eta)\frac{E_\infty - E_0}{E_\infty}\varepsilon_c(t) - \eta\sum_{j=1}^{N_t}\left(\prod_{p=2}^{p+1}\frac{p-\alpha-1}{p}\right)\tilde{\varepsilon}_c(t-j\Delta t) \tag{2.18}$$

where: $\eta = \frac{\tau^\alpha}{\tau^\alpha + \Delta t^\alpha}$; $\Delta t = \frac{t}{N}$ represents the time step and N_t is the maximum number of terms in the Grünwald approximation of $\frac{d^\alpha}{dt^\alpha}$. Note that N_t is strictly less than N.

Following Galucio et al. [19], a fictitious anelastic displacement vector $\{\tilde{u}_c\}$ is defined such that the anelastic strain is expressed as:

$$\tilde{\varepsilon}_c(t) = \left[\tilde{Z}_c\right][D_c]\{\tilde{u}_c(t)\} \tag{2.19}$$

Given the initial conditions, the value of $\{\tilde{u}_c(t)\}$ at time t can be obtained by substituting Eq.

(2.19) into Eq. (2.18). Hence,

$$\{\tilde{u}_c(t)\} = (1-\eta)\frac{E_\infty - E_0}{E_\infty}\{\bar{u}_c(t)\} - \eta\sum_{j=1}^{N_t}\left(\prod_{p=2}^{p+1}\frac{p-\alpha-1}{p}\right)\{\tilde{u}_c(t-j\Delta t)\} \tag{2.20}$$

Combining Eqs. (2.16) and (2.18), the expression of the stress in the core at any time t takes the form:

$$\bar{\sigma}_c(t) = E_0[\zeta]\left[\left(1+\eta\frac{E_\infty - E_0}{E_0}\right)\varepsilon_c(t) + \eta\frac{E_\infty}{E_0}\sum_{j=1}^{N_t}\left(\prod_{p=2}^{p+1}\frac{p-\alpha-1}{p}\right)\tilde{\varepsilon}_c(t-j\Delta t)\right] \tag{2.21}$$

For an elastic material, $\eta = 0$ and $E_0 = E_c$; hence, Eq. (2.21) degenerates into $\bar{\sigma}_c(t) = E_0[\zeta]\varepsilon_c(t) \equiv [Q_c]\varepsilon_c(t)$. Therefore, the constitutive relation of the viscoelastic core is given as:

$$\bar{\sigma}_c(t) = [Q_c]\left[\left(1+\eta\frac{E_\infty - E_0}{E_0}\right)\varepsilon_c(t) + \eta\frac{E_\infty}{E_0}\sum_{j=1}^{N_t}\left(\prod_{p=2}^{p+1}\frac{p-\alpha-1}{p}\right)\tilde{\varepsilon}_c(t-j\Delta t)\right] \tag{2.22}$$

2.3.3 Top Layer (Piezo)

Mechanical

The constitutive relation for three-dimensional piezoelectric ceramics is given by [16] as:

$$\begin{Bmatrix}\sigma_x\\ \sigma_y\\ \sigma_z\\ \tau_{xy}\\ \tau_{yz}\\ \tau_{zx}\end{Bmatrix} = \begin{bmatrix} c_{11} & c_{12} & c_{13} & 0 & 0 & 0\\ c_{12} & c_{22} & c_{23} & 0 & 0 & 0\\ c_{13} & c_{23} & c_{33} & 0 & 0 & 0\\ 0 & 0 & 0 & c_{44} & 0 & 0\\ 0 & 0 & 0 & 0 & c_{55} & 0\\ 0 & 0 & 0 & 0 & 0 & c_{66}\end{bmatrix}\begin{Bmatrix}\epsilon_x\\ \epsilon_y\\ \epsilon_z\\ \gamma_{xy}\\ \gamma_{yz}\\ \gamma_{zx}\end{Bmatrix} - \begin{bmatrix} 0 & 0 & e_{31}\\ 0 & 0 & e_{31}\\ 0 & 0 & e_{33}\\ 0 & e_{15} & 0\\ e_{15} & 0 & 0\\ 0 & 0 & 0\end{bmatrix}\begin{Bmatrix}E_x\\ E_y\\ E_z\end{Bmatrix} \tag{2.23}$$

where E_i represents the electrical field in the $i-th$ direction. The c_{ij} coefficients are the elastic constants in the x, y, and z plane of the piezoelectric material for a given electrical field and the components e_{ij} are the piezoelectric constants. The piezoelectric layer is considered as a beam; hence, stresses in $y-z$ plane are assumed to be zero and $\varepsilon_y = \sigma_z = 0$. Also $E_x = E_y = 0$.

Therefore, Eq. (2.23) reduces to:

$$\begin{cases} \sigma_x &= c_{11}\epsilon_x + c_{13}\epsilon_z - e_{31}E_z \\ 0 &= c_{13}\epsilon_x + c_{33}\epsilon_z - e_{33}E_z \\ \tau_{zx} &= c_{66}\gamma_{zx} \end{cases} \tag{2.24}$$

Isolating ε_z in the second equation and substituting it into the first equation gives:

$$\sigma_p = \begin{Bmatrix} \sigma_x \\ \tau_{zx} \end{Bmatrix} = \begin{Bmatrix} \left(c_{11} - \frac{c_{13}^2}{c_{33}}\right)\epsilon_x - \left(e_{31} - c_{13}\frac{e_{33}}{c_{33}}\right)E_z \\ c_{66}\gamma_{zx} \end{Bmatrix} = \begin{Bmatrix} \overline{c}_{11}\,\epsilon_x - \overline{e}_{31}\,E_z \\ \overline{c}_{66}\,\gamma_{zx} \end{Bmatrix}$$

A compact matrix form is given as:

$$\sigma_p = \begin{bmatrix} \overline{c}_{11} & 0 \\ 0 & \overline{c}_{66} \end{bmatrix} \begin{Bmatrix} \epsilon_x \\ \gamma_{zx} \end{Bmatrix} - \begin{Bmatrix} \overline{e}_{31}E_z \\ 0 \end{Bmatrix} \equiv [Q_p]\varepsilon_p - \begin{Bmatrix} \overline{e}_{31}E_z \\ 0 \end{Bmatrix} \tag{2.25}$$

Electrical

The electrical displacement field D_i is given by [16] as:

$$\begin{Bmatrix} D_x \\ D_y \\ D_z \end{Bmatrix} = \begin{bmatrix} 0 & 0 & 0 & 0 & e_{15} & 0 \\ 0 & 0 & 0 & e_{15} & 0 & 0 \\ e_{31} & e_{31} & e_{33} & 0 & 0 & 0 \end{bmatrix} \begin{Bmatrix} \epsilon_x \\ \epsilon_y \\ \epsilon_z \\ \gamma_{xy} \\ \gamma_{yz} \\ \gamma_{zx} \end{Bmatrix} + \begin{bmatrix} d_{11} & 0 & 0 \\ 0 & d_{22} & 0 \\ 0 & 0 & d_{33} \end{bmatrix} \begin{Bmatrix} 0 \\ 0 \\ E_z \end{Bmatrix}$$

where d_{ij} are the dielectric permittivities at constant strain. For $D_x = D_y = 0$, the transverse electrical displacement field component can be written as:

$$D_z = \left(e_{31} - c_{13}\frac{e_{33}}{c_{33}}\right)\epsilon_x + \left(d_{33} + \frac{e_{33}^2}{c_{33}}\right)E_z \equiv \overline{e}_{31}\epsilon_x + \overline{d}_{33}E_z \tag{2.26}$$

Regrouping Eqs. (2.25) and (2.26) gives:

$$\hat{\sigma}_p = \begin{Bmatrix} \sigma_x \\ \tau_{zx} \\ D_z \end{Bmatrix} = \begin{Bmatrix} \overline{c}_{11}\epsilon_x - \overline{e}_{31}E_z \\ \overline{c}_{66}\gamma_{zx} \\ \overline{e}_{31}\epsilon_x + \overline{d}_{33}E_z \end{Bmatrix} = \begin{bmatrix} \overline{c}_{11} & 0 & -\overline{e}_{31} \\ 0 & \overline{c}_{66} & 0 \\ \overline{e}_{31} & 0 & \overline{d}_{33} \end{bmatrix} \begin{Bmatrix} \epsilon_x \\ \gamma_{zx} \\ E_z \end{Bmatrix} = \begin{bmatrix} \widehat{Q}_p \end{bmatrix} \hat{\varepsilon}_p \tag{2.27}$$

2.4 Variational Formulation

The equation of motion is derived by employing the extended Hamilton's principle [20]:

$$\int_t^{t+\Delta t} (\delta T - \delta U + \delta W) dt = 0 \tag{2.28}$$

where δT and δU are the variation of the kinetic energy and strain energy respectively, and δW is the virtual work done by external forces on the system.

2.4.1 Bottom Layer (Beam)

Kinetic Energy

The variation of the kinetic energy is: $\delta T_b = \int_v \rho_b \delta u_b \ddot{u}_b dv$. Substituting for u_b from Eq. (2.1) yields:

$$\begin{aligned} \delta T_b &= \rho_b \int_x \int_y \{\delta \bar{u}_b\}^T \begin{bmatrix} I_b \end{bmatrix} \{\ddot{\bar{u}}_b\} \, dydx \\ &= \rho_b b \int_x \{\delta \bar{u}_b\}^T \begin{bmatrix} I_b \end{bmatrix} \{\ddot{\bar{u}}_b\} \, dx \end{aligned} \tag{2.29}$$

where the matrix $[I_b]$ is given by:

$$[I_b] = \int_z ([Z_b]^T [Z_b]) dz = \int_z \begin{bmatrix} 1 & z & 0 \\ z & z^2 & 0 \\ 0 & 0 & 1 \end{bmatrix} dz$$

Strain Energy

The variation of the strain energy is: $\delta U_b = \int_v \sigma_b \delta\varepsilon_b dv$. Substituting for σ_b from Eq. (2.13) yields:

$$\delta U_b = \int_v [\bar{Q}_b]\varepsilon_b \delta\varepsilon_b dv$$

and substituting for ε_b from Eq. (2.3) gives the final expression of the variation of the strain energy as:

$$\delta U_b = b\int_x \{\delta\bar{u}_b\}^T \begin{bmatrix} D_b \end{bmatrix}^T \begin{bmatrix} C_b \end{bmatrix} \begin{bmatrix} D_b \end{bmatrix} \begin{Bmatrix} \bar{u}_b \end{Bmatrix} dx \tag{2.30}$$

where the compliance matrix $[C_b]$ of the beam is given by:

$$[C_b] = \int_z ([\tilde{Z}_b]^T[\bar{Q}_b][\tilde{Z}_b])dz = \int_z \begin{bmatrix} \bar{c}_{11} & z\bar{c}_{11} & 0 & 0 \\ z\bar{c}_{11} & z^2\bar{c}_{11} & 0 & 0 \\ 0 & 0 & \bar{c}_{66} & \bar{c}_{66} \\ 0 & 0 & \bar{c}_{66} & \bar{c}_{66} \end{bmatrix} dz$$

2.4.2 Core (Visco)

Kinetic Energy

The variation of the kinetic energy is: $\delta T_c = \int_v \rho_c \delta u_c \ddot{u}_c dv$. A similar use of Eq. (2.4) in place of u_c gives:

$$\begin{aligned} \delta T_c &= \rho_c \int_x \int_y \{\delta\bar{u}_c\}^T \begin{bmatrix} I_c \end{bmatrix} \{\ddot{\bar{u}}_c\}\, dydx \\ &= \rho_c b \int_x \{\delta\bar{u}_c\}^T \begin{bmatrix} I_c \end{bmatrix} \{\ddot{\bar{u}}_c\}\, dx \end{aligned} \tag{2.31}$$

where the matrix $[I_c]$ is given by:

$$[I_c] = \int_z ([Z_c]^T [Z_c]) dz = \int_z \begin{bmatrix} 1 & z & z^2 & z^3 & 0 & 0 & 0 \\ z & z^2 & z^3 & z^4 & 0 & 0 & 0 \\ z^2 & z^3 & z^4 & z^5 & 0 & 0 & 0 \\ z^3 & z^4 & z^5 & z^6 & 0 & 0 & 0 \\ 0 & 0 & 0 & 0 & 1 & z & z^2 \\ 0 & 0 & 0 & 0 & z & z^2 & z^3 \\ 0 & 0 & 0 & 0 & z^2 & z^3 & z^4 \end{bmatrix} dz$$

Strain Energy

The variation of the core strain energy is: $\delta U_c(t) = \int_v \bar{\sigma}_c(t) \delta\varepsilon_c dv$ and is time dependent. Substituting for $\bar{\sigma}_c(t)$ from Eq. (2.22) yields:

$$\begin{aligned} \delta U_c(t) &= \int_v [Q_c] \varepsilon_c(t) \delta\varepsilon_c dv + \int_v [\tilde{Q}_c] \varepsilon_c(t) \delta\varepsilon_c dv + \\ &\quad + \eta \frac{E_\infty}{E_0} \sum_{j=1}^{N_t} \left(\prod_{p=2}^{p+1} \frac{p-\alpha-1}{p} \right) \int_v [Q_c] \tilde{\varepsilon}_c(t - j\Delta t) \delta\varepsilon_c dv \end{aligned} \tag{2.32}$$

where $\left[\tilde{Q}_c\right] = \eta \frac{E_\infty - E_0}{E_0} [Q_c]$. Expanding Eq. (2.32) and substituting for $\varepsilon_c(t)$ and $\tilde{\varepsilon}_c(t - j\Delta t)$ from Eqs. (2.5) and (2.19), Eq. (2.32) can be grouped into the sum $\delta U_c(t) = \delta \bar{U}_c(t) + \delta \tilde{U}_c(t) + \delta \tilde{W}_c(t)$ where,

$$\delta \bar{U}_c(t) = b \int_x \{\delta \bar{u}_c\}^T \left[D_c \right]^T \left[C_c \right] \left[D_c \right] \left\{ \bar{u}_c(t) \right\} dx \tag{2.33}$$

$$\delta \tilde{U}_c(t) = b \int_x \{\delta \bar{u}_c\}^T \left[D_c \right]^T \left[\tilde{C}_c \right] \left[D_c \right] \left\{ \bar{u}_c(t) \right\} dx \tag{2.34}$$

and

$$\delta \tilde{W}_c(t) = \eta \frac{E_\infty}{E_0} \sum_{j=1}^{N_t} \left(\prod_{p=2}^{p+1} \frac{p-\alpha-1}{p} \right) \text{x}$$

$$\text{x } b \int_x \{\delta \bar{u}_c\}^T \left[D_c \right]^T \left[C_c \right] \left[D_c \right] \left\{ \bar{u}_c(t - j\Delta t) \right\} dx \tag{2.35}$$

Eq. (2.33) represents the variation of the elastic strain energy $\delta \bar{U}_c$, Eq. (2.34) is the variation of the anelastic strain energy $\delta \tilde{U}_c$ and Eq. (2.35) is the virtual work done by the induced force in the viscoelastic layer. Here $\left[\tilde{C}_c\right]$ in Eq. (2.34) represents the anelastic compliance matrix of the visco layer and is given by:

$$\left[\tilde{C}_c\right] = \eta \frac{E_\infty - E_0}{E_0} \left[C_c\right] \tag{2.36}$$

where $[C_c]$ denotes the elastic compliance matrix of the viscoelastic layer and is given as:

$$[C_c] = \int_z ([\tilde{Z}_c]^T [Q_c] [\tilde{Z}_c]) dz = \int_{t_2}^{t_6} \begin{bmatrix} [C_c^u] & [0] \\ [0] & [C_c^w] \end{bmatrix} dz$$

where [0] is a 6x6 matrix of zeros and

$$[C_c^u] = \begin{bmatrix} c_{11} & zc_{11} & z^2c_{11} & z^3c_{11} & c_{13} & 2zc_{13} \\ zc_{11} & z^2c_{11} & z^3c_{11} & z^4c_{11} & zc_{13} & 2z^2c_{13} \\ z^2c_{11} & z^3c_{11} & z^4c_{11} & z^5c_{11} & z^2c_{13} & 2z^3c_{13} \\ z^3c_{11} & z^4c_{11} & z^5c_{11} & z^6c_{11} & z^3c_{13} & 2z^4c_{13} \\ c_{13} & zc_{13} & z^2c_{13} & z^3c_{13} & c_{33} & 2zc_{33} \\ 2zc_{13} & 2z^2c_{13} & 2z^3c_{13} & 2z^4c_{13} & 2zc_{33} & 4z^2c_{33} \end{bmatrix}$$

$$[C_c^w] = \begin{bmatrix} c_{66} & 2zc_{66} & 3z^2c_{66} & c_{66} & zc_{66} & z^2c_{66} \\ 2zc_{66} & 4z^2c_{66} & 6z^3c_{66} & 2zc_{66} & 2z^2c_{66} & 2z^3c_{66} \\ 3z^2c_{66} & 6z^3c_{66} & 9z^4c_{66} & 3z^2c_{66} & 3z^3c_{66} & 3z^4c_{66} \\ c_{66} & 2zc_{66} & 3z^2c_{66} & c_{66} & zc_{66} & z^2c_{66} \\ zc_{66} & 2z^2c_{66} & 3z^3c_{66} & zc_{66} & z^2c_{66} & z^3c_{66} \\ z^2c_{66} & 2z^3c_{66} & 3z^4c_{66} & z^2c_{66} & z^3c_{66} & z^4c_{66} \end{bmatrix}$$

2.4.3 Top Layer (Piezo)

Kinetic Energy

Similar to the beam and viscoelastic layers, the variation of the kinetic energy of the piezoelectric layer is: $\delta T_p = \int_v \rho_p \delta u_p \ddot{u}_p dv$. Substituting for u_p from Eq. (2.6) yields:

$$\begin{aligned} \delta T_p &= \rho_p \int_x \int_y \{\delta \bar{u}_b\}^T \left[I_p \right] \{\ddot{\bar{u}}_p\} \, dydx \\ &= \rho_p b \int_x \{\delta \bar{u}_p\}^T \left[I_p \right] \{\ddot{\bar{u}}_p\} \, dx \end{aligned} \tag{2.37}$$

where the matrix $[I_p]$ is given by:

$$[I_p] = \int_z ([Z_p]^T [Z_p]) dz = \int_z \begin{bmatrix} 1 & z & 0 \\ z & z^2 & 0 \\ 0 & 0 & 1 \end{bmatrix} dz$$

Strain Energy

The variation of the strain energy in the piezoelectric layer is: $\delta \hat{U}_p = \int_v \hat{\sigma}_p \delta \hat{\varepsilon}_p dv$. Substituting for $\hat{\sigma}_p$ from Eq. (2.27) yields:

$$\delta \hat{U}_p = \int_v [\hat{Q}_p] \hat{\varepsilon}_p \delta \hat{\varepsilon}_p dv = \int_v \begin{Bmatrix} \delta \epsilon_x \\ \delta \gamma_{zx} \\ \delta E_z \end{Bmatrix}^T \begin{bmatrix} \overline{c}_{11} & 0 & -\overline{e}_{31} \\ 0 & \overline{c}_{66} & 0 \\ \overline{e}_{31} & 0 & \overline{d}_{33} \end{bmatrix} \begin{Bmatrix} \epsilon_x \\ \gamma_{zx} \\ E_z \end{Bmatrix} dv \tag{2.38}$$

Actuation

The actuator configuration is characterized by the application of a constant electrical field to the piezoelectric ceramics. The electrical field is a function of voltage (i.e. Eq. (2.11)), which represents an external force applied to the system. Given that E_z is known, $\delta E_z = 0$. Hence, Eq. (2.38) reduces to

$$\delta\hat{U}_p = \int_v \left[\begin{Bmatrix} \delta\epsilon_x \\ \delta\gamma_{zx} \end{Bmatrix}^T \begin{bmatrix} \bar{c}_{11} & 0 \\ 0 & \bar{c}_{66} \end{bmatrix} \begin{Bmatrix} \epsilon_x \\ \gamma_{zx} \end{Bmatrix} - \begin{Bmatrix} \delta\epsilon_x \\ \delta\gamma_{zx} \end{Bmatrix}^T \begin{Bmatrix} \bar{e}_{31}E_z \\ 0 \end{Bmatrix} \right] dv$$

$$\delta\hat{U}_p = \int_v \left[\delta\varepsilon_p{}^T [Q_p] \varepsilon_p - \delta\varepsilon_p{}^T \begin{Bmatrix} \bar{e}_{31}E_z \\ 0 \end{Bmatrix} \right] dv \tag{2.39}$$

The above equation can be separated and rewritten as $\delta\hat{U}_p = \delta U_p + \delta\hat{W}_p$,

where $\delta U_p = \int_v \delta\varepsilon_p{}^T [Q_p] \varepsilon_p \, dv$ denotes the mechanical strain energy in the piezoelectric ceramics and $\delta\hat{W}_p = -\int_v \delta\varepsilon_p{}^T \begin{Bmatrix} \bar{e}_{31}E_z & 0 \end{Bmatrix}^T dv$ is the virtual work done by the electrical force which arises from the applied electrical field E_z. Substituting for ε_p from Eq. (2.8) gives the expressions for δU_p and $\delta\hat{W}_p$ in expanded forms as:

$$\delta U_p = b \int_x \{\delta\bar{u}_p\}^T \begin{bmatrix} D_p \end{bmatrix}^T \begin{bmatrix} C_p \end{bmatrix} \begin{bmatrix} D_p \end{bmatrix} \begin{Bmatrix} \bar{u}_p \end{Bmatrix} dx \tag{2.40}$$

$$\delta\hat{W}_p = -b \int_x \{\delta\bar{u}_p\}^T \begin{bmatrix} D_p \end{bmatrix}^T \begin{bmatrix} \tilde{Z}_p \end{bmatrix}^T \begin{Bmatrix} \bar{e}_{31}E_z \\ 0 \end{Bmatrix} dx \tag{2.41}$$

where the compliance matrix $[C_p]$ is given as:

$$[C_p] = \int_z ([\tilde{Z}_p]^T [\bar{Q}_p] [\tilde{Z}_p]) dz = \int_z \begin{bmatrix} \bar{c}_{11} & z\bar{c}_{11} & 0 & 0 \\ z\bar{c}_{11} & z^2\bar{c}_{11} & 0 & 0 \\ 0 & 0 & \bar{c}_{66} & \bar{c}_{66} \\ 0 & 0 & \bar{c}_{66} & \bar{c}_{66} \end{bmatrix} dz$$

Chapter 3

Finite Element Modeling

A typical finite element of the composite structure is shown in Fig. 3.1. Seven locations are

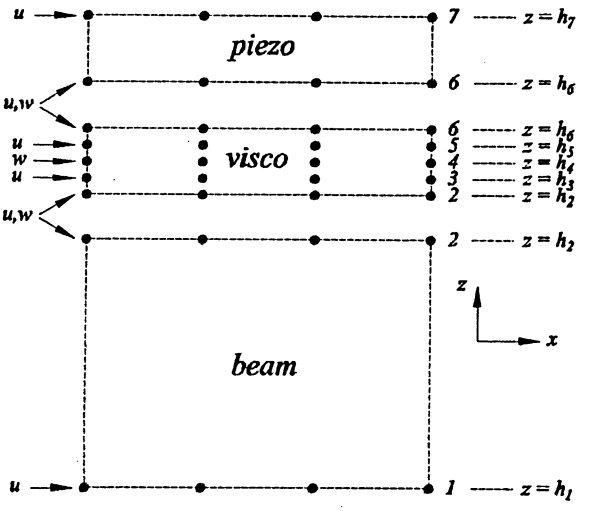

Figure 3.1: Schematic of a finite element

selected through the thickness and their position relative to the geometric mid-surface are $t_1, t_2, \ldots, t_7$. Four nodes are defined along the span to permit a cubic Lagrange interpolation [21] of the fields variable. The global displacement vector of an element is given by:

$$u^T = \{\ u_1 \quad u_2 \quad w_2 \quad u_3 \quad w_4 \quad u_5 \quad u_6 \quad w_6 \quad u_7\ \} \tag{3.1}$$

where u_i and w_i denote the magnitudes of the axial and transverse displacements evaluated at the $i-th$ location through the thickness where applicable.

Each node has nine degrees of freedom. Therefore, the elemental displacement vector q_e contains 36 degrees of freedom and is defined as:

$$q_e^T = \{u_{11}\ u_{21}\ w_{21}\ u_{31}\ w_{41}\ u_{51}\ u_{61}\ w_{61}\ u_{71} \ldots u_{14}\ u_{24}\ w_{24}\ u_{34}\ w_{44}\ u_{54}\ u_{64}\ w_{64}\ u_{74}\}$$

where the first index $i = 1 \ldots 7$ represents the through thickness displacement and the second index $j = 1 \ldots 4$ represents the node along the span.

3.1 Mapping

Here, the coefficients of the field variables in each layer, as expressed in Chapter 2, are now written in terms of their appropriate displacement field vectors.

3.1.1 Bottom Layer (Beam)

The transformation through the thickness of the displacement vector is expressed in matrix form as:

$$\begin{Bmatrix} u_1 \\ u_2 \\ w_2 \end{Bmatrix} = \begin{bmatrix} 1 & t_1 & 0 \\ 1 & t_2 & 0 \\ 0 & 0 & 1 \end{bmatrix} \begin{Bmatrix} a_0 \\ a_1 \\ l_0 \end{Bmatrix}$$

Solving for a_0, a_1 and l_0, the resulting expression gives

$$\begin{Bmatrix} a_0 \\ a_1 \\ l_0 \end{Bmatrix} = \begin{bmatrix} 1 & t_1 & 0 \\ 1 & t_2 & 0 \\ 0 & 0 & 1 \end{bmatrix}^{-1} \begin{Bmatrix} u_1 \\ u_2 \\ w_2 \end{Bmatrix} \equiv \{\bar{u}_b\} = [T_b] \begin{Bmatrix} u_1 \\ u_2 \\ w_2 \end{Bmatrix} \tag{3.2}$$

3.1.2 Core (Visco)

For the core, the transformation through the thickness of the axial and transverse displacement can be partitioned and given as:

$$\begin{Bmatrix} u_2 \\ u_3 \\ u_5 \\ u_6 \end{Bmatrix} = \begin{bmatrix} 1 & t_2 & t_2^2 & t_2^3 \\ 1 & t_3 & t_3^2 & t_3^3 \\ 1 & t_5 & t_5^2 & t_5^3 \\ 1 & t_6 & t_6^2 & t_6^3 \end{bmatrix} \begin{Bmatrix} c_0 \\ c_1 \\ c_2 \\ c_3 \end{Bmatrix}$$

Performing the inversion operation, the above relation gives,

$$\begin{Bmatrix} c_0 \\ c_1 \\ c_2 \\ c_3 \end{Bmatrix} = \begin{bmatrix} 1 & t_2 & t_2^2 & t_2^3 \\ 1 & t_3 & t_3^2 & t_3^3 \\ 1 & t_5 & t_5^2 & t_5^3 \\ 1 & t_6 & t_6^2 & t_6^3 \end{bmatrix}^{-1} \begin{Bmatrix} u_2 \\ u_3 \\ u_5 \\ u_6 \end{Bmatrix} = [T_u] \begin{Bmatrix} u_2 \\ u_3 \\ u_5 \\ u_6 \end{Bmatrix} \tag{3.3}$$

for the transverse displacement,

$$\begin{Bmatrix} w_2 \\ w_4 \\ w_6 \end{Bmatrix} = \begin{bmatrix} 1 & t_2 & t_2^2 \\ 1 & t_4 & t_4^2 \\ 1 & t_6 & t_6^2 \end{bmatrix} \begin{Bmatrix} m_0 \\ m_1 \\ m_2 \end{Bmatrix}$$

and the inversion gives:

$$\begin{Bmatrix} m_0 \\ m_1 \\ m_2 \end{Bmatrix} = \begin{bmatrix} 1 & t_2 & t_2^2 \\ 1 & t_4 & t_4^2 \\ 1 & t_6 & t_6^2 \end{bmatrix}^{-1} \begin{Bmatrix} w_2 \\ w_4 \\ w_6 \end{Bmatrix} = [T_w] \begin{Bmatrix} w_2 \\ w_4 \\ w_6 \end{Bmatrix} \tag{3.4}$$

Eqs. (3.3) and (3.4) are combined and expressed as:

$$\begin{Bmatrix} c_0 \\ c_1 \\ c_2 \\ c_3 \\ m_0 \\ m_1 \\ m_2 \end{Bmatrix} = \begin{bmatrix} [T_u] & [0] \\ [0]^T & [T_w] \end{bmatrix} \begin{Bmatrix} u_2 \\ u_3 \\ u_5 \\ u_6 \\ w_2 \\ w_4 \\ w_6 \end{Bmatrix} \equiv \{\bar{u}_c\} = [T_c] \begin{Bmatrix} u_2 \\ u_3 \\ u_5 \\ u_6 \\ w_2 \\ w_4 \\ w_6 \end{Bmatrix} \tag{3.5}$$

where [0] is a 4x3 matrix of zeros.

3.1.3 Top Layer (Piezo)

Identical to the bottom layer, the transformation through the thickness of the displacement vector takes the form:

$$u_p = \begin{Bmatrix} u_6 \\ w_6 \\ u_7 \end{Bmatrix} = \begin{bmatrix} 1 & t_6 & 0 \\ 0 & 0 & 1 \\ 1 & t_7 & 0 \end{bmatrix} \begin{Bmatrix} e_0 \\ e_1 \\ n_0 \end{Bmatrix}$$

Hence,

$$\begin{Bmatrix} e_0 \\ e_1 \\ n_0 \end{Bmatrix} = \begin{bmatrix} 1 & t_6 & 0 \\ 0 & 0 & 1 \\ 1 & t_7 & 0 \end{bmatrix}^{-1} \begin{Bmatrix} u_6 \\ w_6 \\ u_7 \end{Bmatrix} \equiv \{\bar{u}_p\} = [T_p] \begin{Bmatrix} u_6 \\ w_6 \\ u_7 \end{Bmatrix} \tag{3.6}$$

3.2 Shape Functions

The field variable are interpolated along the span using cubic Lagrange interpolation shape functions [21] which are given as:

$$\left.\begin{aligned} N_{1\xi} &= -\frac{(3\xi+1)(3\xi-1)(\xi-1)}{16} \\ N_{2\xi} &= \frac{9(\xi+1)(3\xi-1)(\xi-1)}{16} \\ N_{3\xi} &= -\frac{9(\xi+1)(3\xi+1)(\xi-1)}{16} \\ N_{4\xi} &= \frac{(\xi+1)(3\xi+1)(3\xi-1)}{16} \end{aligned}\right\} -1 \le \xi \le 1 \tag{3.7}$$

3.2.1 Bottom Layer (Beam)

The displacement vector $u_b = \{u_1 \; u_2 \; w_2\}^T$ is expanded as:

$$u_b = \begin{Bmatrix} u_1 \\ u_2 \\ w_2 \end{Bmatrix} = \begin{bmatrix} N_{b1} & N_{b2} & N_{b3} & N_{b4} \end{bmatrix} q_e = \begin{bmatrix} N_b \end{bmatrix} q_e \tag{3.8}$$

where,

$$[N_{bi}] = \begin{bmatrix} N_{i\xi} & 0 & 0 & 0 & 0 & 0 & 0 & 0 & 0 \\ 0 & N_{i\xi} & 0 & 0 & 0 & 0 & 0 & 0 & 0 \\ 0 & 0 & N_{i\xi} & 0 & 0 & 0 & 0 & 0 & 0 \end{bmatrix}$$

Substituting for u_b from Eq. (3.8) into Eq. (3.2) yields

$$\{\bar{u}_b\} = [T_b][N_b]q_e \tag{3.9}$$

Substituting for $\{\bar{u}_b\}$ from Eq. (3.9) into Eqs. (2.29) and (2.30). The variation of the resulting kinetic and strain energy in the bottom layer gives:

$$\delta T_b = \delta q_e^T \left[\rho_b b \int_{-1}^{1} [N_b]^T [T_b]^T [I_b][T_b][N_b] J(\xi) d\xi\right] \ddot{q}_e = \delta q_e^T [M_b] \ddot{q}_e \tag{3.10}$$

and

$$\begin{aligned} \delta U_b &= \delta q_e^T \left[b \int_{-1}^{1} [N_b]^T [T_b]^T [D_b]^T [C_b][D_b][T_b][N_b]|J| d\xi \right] q_e \\ &= \delta q_e^T \left[b \int_{-1}^{1} [B_b]^T [C_b][B_b]|J| d\xi \right] q_e \equiv \delta q_e^T [K_b] q_e \end{aligned} \tag{3.11}$$

where $|J|$ is the jacobian.

3.2.2 Core (Visco)

The displacement vector $u_c = \{u_2\ u_3\ w_5\ u_6\ w_2\ w_4\ w_6\}^T$ can be expanded as:

$$u_c = \left[\begin{array}{cccc} N_{c1} & N_{c2} & N_{c3} & N_{c4} \end{array} \right] q_e = \left[N_c \right] q_e \tag{3.12}$$

where

$$[N_{ci}] = \begin{bmatrix} 0 & N_{i\xi} & 0 & 0 & 0 & 0 & 0 & 0 & 0 \\ 0 & 0 & 0 & N_{i\xi} & 0 & 0 & 0 & 0 & 0 \\ 0 & 0 & 0 & 0 & 0 & N_{i\xi} & 0 & 0 & 0 \\ 0 & 0 & 0 & 0 & 0 & 0 & N_{i\xi} & 0 & 0 \\ 0 & 0 & N_{i\xi} & 0 & 0 & 0 & 0 & 0 & 0 \\ 0 & 0 & 0 & 0 & N_{i\xi} & 0 & 0 & 0 & 0 \\ 0 & 0 & 0 & 0 & 0 & 0 & 0 & N_{i\xi} & 0 \end{bmatrix}$$

Substituting for u_c from Eq. (3.12) into Eq. (3.5) yields:

$$\{\bar{u}_c\} = [T_c][N_c] q_e \tag{3.13}$$

Similarly the anelastic displacement can be written as:

$$\{\tilde{u}_c\} = [T_c][N_c] \tilde{q}_e \tag{3.14}$$

For a given time t, $\tilde{q}_e(t)$ can be computed by substituting Eq. (3.14) into Eq. (2.20) to obtain a similar expression as in Ref. [19] and given as:

$$\tilde{q}_e(t) = (1-\eta)\frac{E_\infty - E_0}{E_\infty}\bar{q}_e(t) - \eta\sum_{j=1}^{N_t}\left(\prod_{p=2}^{p+1}\frac{p-\alpha-1}{p}\right)\tilde{q}_e(t-j\Delta t) \tag{3.15}$$

Substituting for $\{\bar{u}_c\}$ from Eq. (3.13) into Eqs. (2.31) and (2.33) gives the variation of the kinetic and elastic strain energy in the core as:

$$\delta T_c = \delta q_e^T\left[\rho_c b\int_{-1}^{1}[N_c]^T[T_c]^T[I_c][T_c][N_c]|J|d\xi\right]\ddot{q}_e = \delta q_e^T[M_c]\ddot{q}_e \tag{3.16}$$

and

$$\begin{aligned}\delta\bar{U}_c(t) &= \delta q_e^T\left[b\int_{-1}^{1}[N_c]^T[T_c]^T[D_c]^T[C_c][D_c][T_c][N_c]|J|d\xi\right]q_e(t)\\ &= \delta q_e^T\left[b\int_{-1}^{1}[B_c]^T[C_c][B_c]|J|d\xi\right]q_e(t) \equiv \delta q_e^T[K_c]q_e(t)\end{aligned} \tag{3.17}$$

Similarly, the expression of the variation of the anelastic strain energy is found by substituting for $\{\bar{u}_c\}$ from Eq. (3.13) into Eq. (2.34). Hence

$$\begin{aligned}\delta\tilde{U}_c(t) &= \delta q_e^T\left[b\int_{-1}^{1}[N_c]^T[T_c]^T[D_c]^T[\tilde{C}_c][D_c][T_c][N_c]|J|d\xi\right]q_e(t)\\ &= \delta q_e^T\left[b\int_{-1}^{1}[B_c]^T[\tilde{C}_c][B_c]|J|d\xi\right]q_e(t) \equiv \delta q_e^T[\tilde{K}_c]q_e(t)\end{aligned} \tag{3.18}$$

Finally, using Eq. (3.14) in Eq. (2.35) yields the expression of the virtual work done by the induced force in the viscoelastic layer as:

$$\begin{aligned}\delta\tilde{W}_c(t) &= \delta q_e^T\eta\frac{E_\infty}{E_0}\left[b\int_{-1}^{1}[B_c]^T[C_c][B_c]|J|d\xi\right]\sum_{j=1}^{N_t}\left(\prod_{p=2}^{p+1}\frac{p-\alpha-1}{p}\right)\tilde{q}_e(t-j\Delta t)\\ &= \delta q_e^T\eta\frac{E_\infty}{E_0}[K_c]\sum_{j=1}^{N_t}\left(\prod_{p=2}^{p+1}\frac{p-\alpha-1}{p}\right)\tilde{q}_e(t-j\Delta t) = \delta q_e^T\tilde{F}_c(t)\end{aligned} \tag{3.19}$$

3.2.3 Top Layer (Piezo)

Similar to the bottom layer, the displacement vector $u_p = \{u_6\ w_6\ u_7\}^T$ is expanded as:

$$u_p = \left\{ \begin{array}{c} u_6 \\ w_6 \\ u_7 \end{array} \right\} = \left[\begin{array}{cccc} N_{p1} & N_{p2} & N_{p3} & N_{p4} \end{array} \right] q_e = \left[\begin{array}{c} N_p \end{array} \right] q_e \tag{3.20}$$

where

$$[N_{pi}] = \left[\begin{array}{ccccccccc} 0 & 0 & 0 & 0 & 0 & 0 & N_{i\xi} & 0 & 0 \\ 0 & 0 & 0 & 0 & 0 & 0 & 0 & N_{i\xi} & 0 \\ 0 & 0 & 0 & 0 & 0 & 0 & 0 & 0 & N_{i\xi} \end{array} \right]$$

Hence, substituting for u_p from Eq. (3.20) into Eq. (3.6) yields:

$$\{\bar{u}_p\} = [T_p][N_p]q_e \tag{3.21}$$

Substituting for $\{\bar{u}_p\}$ from Eq. (3.21) into Eqs. (2.37), (2.40) and (2.41). The variation of the resulting kinetic, strain energy and virtual work in piezoelectric layer gives:

$$\delta T_p = \delta q_e^T \left[\rho_p b \int_{-1}^{1} [N_p]^T [T_p]^T [I_p][T_p][N_p]|J|d\xi \right] \ddot{q}_e = \delta q_e^T [M_p] \ddot{q}_e \tag{3.22}$$

$$\begin{aligned} \delta U_p &= \delta q_e^T \left[b \int_{-1}^{1} [N_p]^T [T_p]^T [D_p]^T [C_p][D_p][T_p][N_p]|J|d\xi \right] q_e \\ &= \delta q_e^T \left[b \int_{-1}^{1} [B_p]^T [C_p][B_p]|J|d\xi \right] q_e \equiv \delta q_e^T [K_p] q_e \end{aligned} \tag{3.23}$$

$$\begin{aligned} \delta \hat{W}_p &= \delta q_e^T \left[-b \int_{-1}^{1} [N_p]^T [T_p]^T [D_p]^T [\tilde{Z}_p] \left\{ \begin{array}{c} \bar{e}_{31} E_z \\ 0 \end{array} \right\} |J|d\xi \right] \\ &= \delta q_e^T \left[-b \int_{-1}^{1} [B_p]^T [\tilde{Z}_p] \left\{ \begin{array}{c} \bar{e}_{31} E_z \\ 0 \end{array} \right\} |J|d\xi \right] \equiv \delta q_e^T \hat{F}_p \end{aligned} \tag{3.24}$$

The virtual work due to an external load F_e applied at a given position ξ_f on an element is given as:

$$\delta W_e = \delta q_e^T F_e \int_{-1}^{1} [N]^T \mathcal{M}^T \delta(\xi - \xi_f) d\xi \tag{3.25}$$

where $[N] = \begin{bmatrix} N_{1\xi}I & N_{2\xi}I & N_{3\xi}I & N_{4\xi}I \end{bmatrix}$, with I being a 9x9 identity matrix and $\mathcal{M} = [0\,0\,0\,0\,0\,0\,0\,1\,0]$ is a boolean mapping vector.

To evaluate the integrals in equations (3.10), (3.11), (3.16), (3.17), (3.18), (3.19), (3.22), (3.23), (3.24) and (3.25), a standard four points Gaussian quadrature is adopted [14], [21] and [22].

3.3 Equation of Motion

At time t, using the extended Hamilton's principle (i.e Eq. (2.28)), the element governing equation is derived and given as:

$$([M_b] + [M_c] + [M_p])\,\ddot{q}_e(t) + \left([K_b] + [K_c] + [\tilde{K}_c] + [K_p]\right) q_e(t) = F_e(t) + \tilde{F}_c(t) + \hat{F}_p(t) \tag{3.26}$$

It is worth mentioning, and as observed in [19], that the introduction of a viscoelastic material augments the element governing equation with both stiffness and force modulators which expression are given by:

$$\left[\tilde{K}_c\right] = \eta \frac{E_\infty - E_0}{E_0} [K_c] \tag{3.27}$$

and

$$\tilde{F}_c(t) = -\eta \frac{E_\infty}{E_0} [K_c] \sum_{j=1}^{N_t} \left(\prod_{p=2}^{p+1} \frac{p - \alpha - 1}{p} \right) \tilde{q}_e(t - j\Delta t) \tag{3.28}$$

The global system equation is obtained following the methods of finite element technique [21] by assembling the element contributions over the entire domain. This equation is written as:

$$[\boldsymbol{M}]\ddot{\boldsymbol{q}}(t) + [\boldsymbol{K}]\boldsymbol{q}(t) = \boldsymbol{F}(t) + \tilde{\boldsymbol{F}}(t) + \hat{\boldsymbol{F}}(t) \tag{3.29}$$

where $[\boldsymbol{M}]$, $[\boldsymbol{K}]$, $\boldsymbol{F}$, $\tilde{\boldsymbol{F}}$ and $\hat{\boldsymbol{F}}$ represent the global mass matrix, stiffness matrix, external force vector, viscoelastic force modulation vector and electrical force vector, respectively.

The Newmark time-integration scheme [21, 23] is adopted to solve the resulting governing equation. This classical algorithm has been modified to account for the viscoelastic properties. A new parameter is introduced for the storage of the anelastic displacement history.

Chapter 4

Numerical Simulation

4.1 Validation

The current formulation is validated by revisiting three problems that were examined in the literature. The first problem involves the static analysis of a sandwich beam. The second problem pertains to the frequency analysis of a sandwich beam with a soft core, and the third, the dynamic analysis of a sandwich beam with a viscoelastic core.

4.1.1 Piezo-Aluminium Sandwich Beam

This problem was first analyzed by Zhang and Sun [16] using an analytical method. Later, Galucio et al. [18] studied the same problem using finite element analysis with piecewise linear displacements and a partial continuity formulation. The system is a cantilever sandwich beam composed of an aluminium core covered by piezoelectric faces Fig. 4.1. Both piezoelectric faces are actuators and a voltage of $10V$ is applied. The mechanical properties of the the

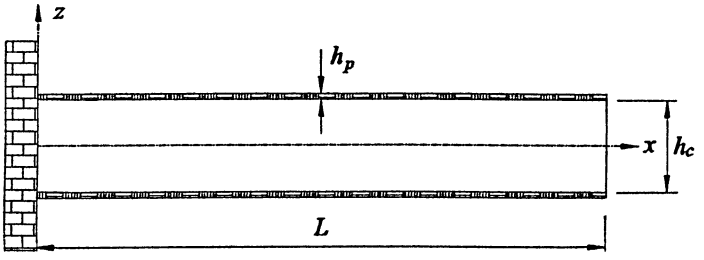

Figure 4.1: Piezo-Aluminium Sandwich beam

aluminium core and the piezoelectric faces are given in Table 4.1.

Table 4.1: Mechanical Properties of piezo-aluminium sandwich beam.

PZT5H						Aluminium	
GPa				Cm^{-2}		GPa	ν
c_{11}	c_{13}	c_{33}	c_{66}	e_{31}	e_{33}	E	
126	84.1	117	23	-6.5	23.3	70.3	0.345

The dimension of the sandwich beam are: $L = 100\,mm$ (length of the beam), $h_c = 16\,mm$ (thickness of the aluminium core) and $h_p = 1\,mm$ (thickness of the piezoelectric faces). Convergence of the solution is obtained using 5 finite elements.

The results for a fully cantilevered boundary condition for both the current and conventional formulation are depicted in Fig. 4.2 (transverse displacement along the beam length) and Fig. 4.3 (axial stress at midpoint of the beam). These results are in good agreement with the results of [16] and [18] in which the conventional formulation method is employed.

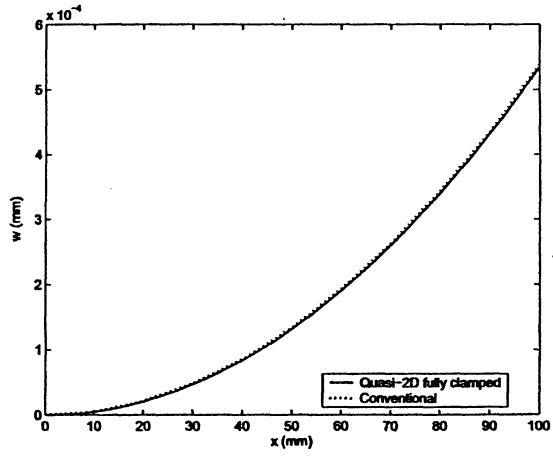

Figure 4.2: Transverse Displacement along the span of the beam

A modification to the problem is now introduced in order to demonstrate the superiority of the quasi-two-dimensional formulation over the conventional formulation. Here, the geometric properties are unchanged while the piezoelectric faces are replaced with aluminium and the core is an elastic material with a Young's modulus that is a fraction of that of the face-sheets: $E_c = \alpha E$ where $\alpha = 0.0015$; $\nu_c = 0.495$. A point load of $1N$ is applied downward at the free end. The axial stress distribution in the core only is plotted in Fig. 4.4. Two boundaries

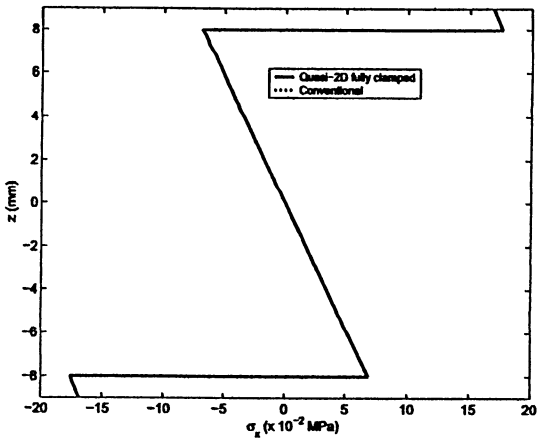

Figure 4.3: Through-the-thickness Axial Stress Distribution at mid-span of the beam

conditions are examined for the quasi-two-dimensional formulation: fully cantilevered and partially cantilevered. In the former, one end of the face-sheets and core is clamped, while only the end of the face-sheets is clamped in the latter. The nature of the conventional sandwich beam formulation is such that only the fully cantilevered boundary conditions are examinable.

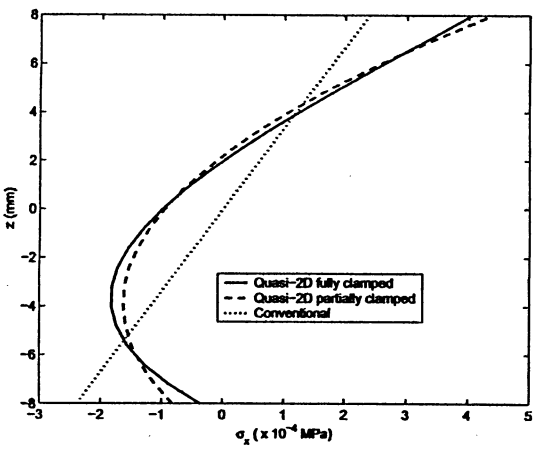

Figure 4.4: Through-the-thickness Axial Stress distribution in the core ($h_c = 16\,mm$).

The results show a dependency in both the formulation and boundary conditions. The limitation of the conventional formulation for the soft core is also revealed, but this, as expected, is more pronounce with increasing core thickness. For example, Figs. 4.5 and 4.6 depict the axial stress distribution in the core for the core thickness of $10\,mm$ and $4\,mm$ respectively.

While the difference in the core axial stress obtained using the present and conventional formulations increases with the core thickness, the difference in the deflection of the beam increases with the decreasing core thickness (see Fig. 4.7).

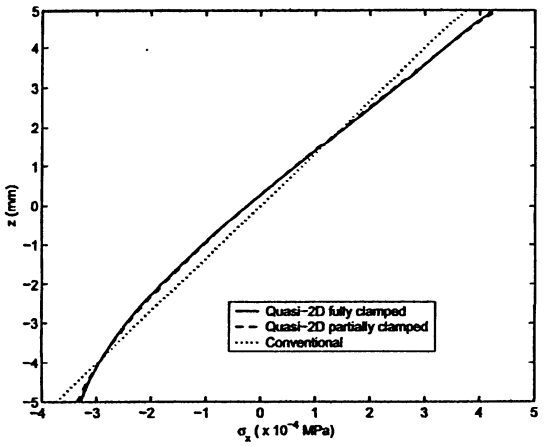

Figure 4.5: Through-the-thickness Axial Stress distribution in the core ($h_c = 10\,mm$).

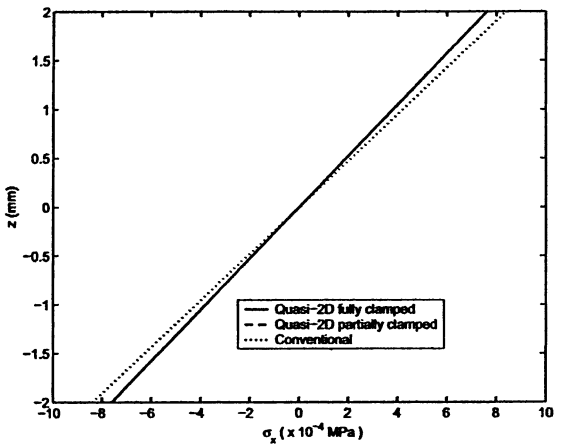

Figure 4.6: Through-the-thickness Axial Stress distribution in the core ($h_c = 4\,mm$).

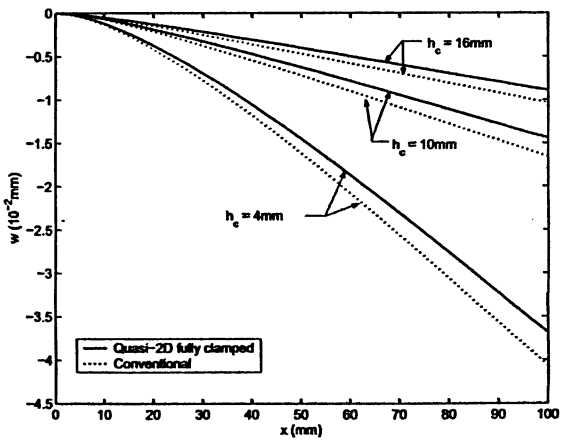

Figure 4.7: Deflection for Various values of core thickness (h_c)

The transverse displacement obtained using the current formulation are independent of boundary conditions.

4.1.2 Sandwich Beam with Soft Core

The effectiveness of the current formulation in the free vibration response of a soft core sandwich beam is presented by comparing the presently obtained natural frequencies with those obtained using the conventional formulation, the consistent higher-order dynamic equations of Sokolinsky and Nutt [24], and a two-dimensional finite element analysis using commercial software NASTRAN and ABAQUS [25].

The cantilevered sandwich beam is composed of a soft core Divinycell H60 and steel facesheets. The geometric properties of the beam are: $L = 260\ mm$ (length), $b = 59.9\ mm$ (width), $h_a = h_b = 1.9\,mm$ (thickness of the top and bottom layer respectively), $h_c = 34.8\,mm$ (core thickness). The mechanical properties are given in Table 4.2.

Table 4.2: Mechanical Properties of soft core-steel sandwich beam.

Divinycell H60 (core)				Steel (face sheets)			
GPa		kgm^{-3}	ν	GPa		kgm^{-3}	ν
E	G	ρ		E	G	ρ	
0.056	0.022	60	0.27	210	81	7900	0.30

The results are tabulated in Table 4.3 and they show that the frequencies from the current formulation and the two-dimensional finite element are quite similar. For comparison, the results from Ref. [25] were achieved using 7 elements through the thickness and 130 elements along the span for a total of 3005 nodes, which represent approximately 7000 degrees of freedom. The quasi-two-dimensional formulation uses 10 elements along the span, which translates to 31 nodes and 217 degrees of freedom.

Combining both experimental and analytical studies, Sokolinsky et al. [25] showed that the first five modes and the 10-th mode correspond to antisymmetric modes i.e., the face sheets and the core are moving in the same direction. This mean that there is less tension/compression in the core but more shear. It can be noticed that for these modes the error with the conventional formulation is less pronounce. Modes 6-8 correspond to the symmetric modes where the facesheets move in opposite directions symmetric to the core. Note that the quasi-two-dimensional formulation (i.e. the current formulation) results are in better agreement with the FEM results

than the results with both the conventional and the consistent higher order formulation.

It is obvious that for the symmetric mode to occur, the core has to be compressible which is not assumed in the conventional models. Thus the limitation of the formulation for soft-core sandwich structure.

Table 4.3: Comparison of first 10 natural frequencies.

Mode	*Convent.*	*Consist.* *Ref.* [24]	*FEM* *Ref.* [25]	Quasi 2D (Present Method)	
				Fully Clamped	*Partially Clamped*
1	154	165	165	165	165
2	437	512	512	513	512
3	680	912	913	915	914
4	898	1378	1379	1384	1381
5	1124	1940	1939	1947	1944
6	1356	2392	2476	2483	2483
7	1593	2395	2509	2508	2508
8	1832	2425	2558	2554	2553
9	2073	2524	2567	2582	2571
10	2315	2612	2608	2623	2619

4.1.3 Visco-Aluminium Sandwich Beam

The final example to demonstrate the effectiveness of the current formulation for viscoelastic core is from the work of Galucio et al. [19]. The composite beam has a viscoelastic core that is covered with two layers of aluminium. (see Fig. 4.8). The load is applied through the form

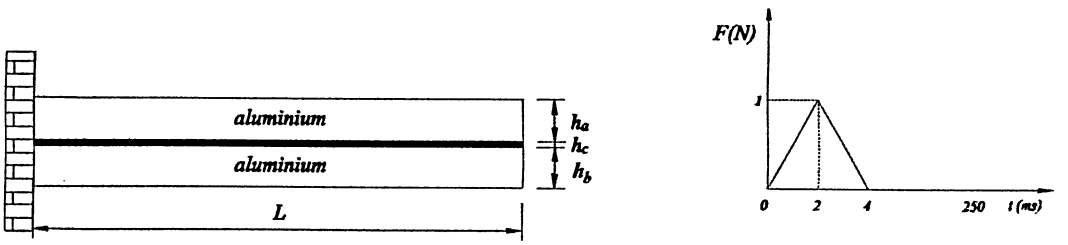

Figure 4.8: Visco-Aluminium Sandwich beam and Load

of a triangular impulse acting on the free end of the beam for 4 ms and then released. The observation time is 250 ms. The geometric properties of the beam are: $L = 200\,mm$ (length), $b = 10\,mm$ (width), $h_a = h_b = 1\,mm$ (thickness of the top and bottom layer respectively),

$h_c = 0.2\,mm$ (core thickness). The parameters of the fractional derivative model are: $\alpha = 0.7915$ and $\tau = 1.4052 \text{ x } 10^{-2}\,ms$. The time step $\Delta t = 0.25\,ms$ and the mechanical properties are tabulated in Table 4.4.

Table 4.4: Mechanical Properties of Visco-Aluminium sandwich beam.

ISD112 (at 27° C)				Aluminium		
MPa		kgm^{-3}	ν	GPa	kgm^{-3}	ν
E_o	E_∞	ρ		E	ρ	
1.5	69.9495	1600	0.5	70.3	2690	0.345

The tip transverse displacement history is depicted in Fig. 4.9. Following the observation in the static and free-vibration scenarios, the tip displacement is independent of the boundary condition. The conventional formulation shows a faster damping of the transverse displacement magnitude, and there is a phase shift between the two formulations.

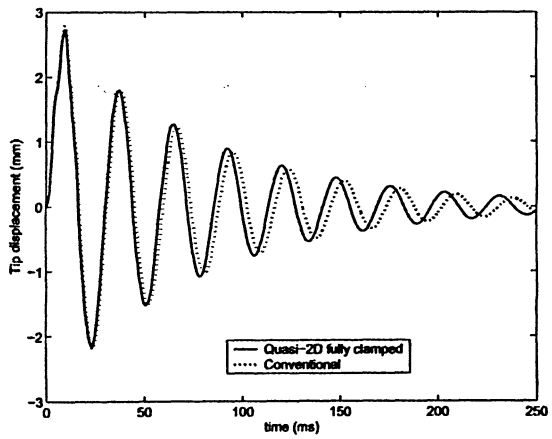

Figure 4.9: Dynamic Response of The Viscoelastic Sandwich beam

4.2 Sample Simulation

Two examples of a cantilever constrained layer beams are considered in this section. In the first, the span of the host beam is entirely covered with a viscoelastic layer which, in turn, is covered by a piezoelectric layer. The viscoelastic and piezoelectric layers cover section of the span measured from the free end in the second scenario. The excitation force is applied at the free end, and it is either a harmonic force or a triangular impulse load as depicted in Fig. 4.8.

The geometric characteristics of the composite beam are: $L = 300\,mm$ (length of the beam), $b = 15\ mm$ (width of the beam) $h_b = 3\,mm$ (thickness of the elastic layer), $h_c = 0.2\,mm$ (thickness of the viscoelastic layer) and $h_p = 1\,mm$ (thickness of the piezoelectric layer). The number of terms in the Grünwald approximation of the fractional derivative $N = 1000$. The mechanical properties of any given layer are listed in Tables 4.1 and 4.4. The density of the piezoelectric layer is $\rho_p = 7500\,kg/m^3$. A simple velocity feedback is adopted for the controlled vibrations. The observation time of the beam subjected to a triangular load is *1 second* and *2.5 second* for the harmonic load.

4.2.1 Case of fully constrained layer beam

In this scenario, the elastic layer or the host beam is entirely covered with the viscoelastic layer and piezoelectric layer Fig. 4.10. The beam is meshed with five finite elements along

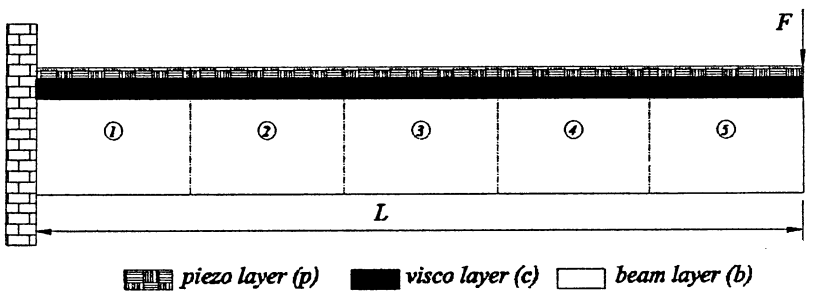

Figure 4.10: Schematic of a fully constrained layer beam

the span. The gain $K_v = 150\,Vs\,/\,m$. The results obtained with the triangular impulse load and with the harmonic load are illustrated in Figs. 4.11 and 4.12, respectively. Each figure depicts the uncontrolled and controlled tip deflection and the actuation voltage applied when the piezoelectric layer is actuating. Damping in the uncontrolled scenario is passive - solely from the viscoelastic layer.

The effectiveness of the active-passive damping combination over sole employment of passive damping is readily observable by comparing Figs. 4.11(a) and 4.11(b) on the one hand, and Figs. 4.12(a) and 4.12(b) on the other hand. It is also worth mentioning that the magnitudes of the actuating voltages as depicted in Figs. 4.11(c) and 4.12(c) are far removed from

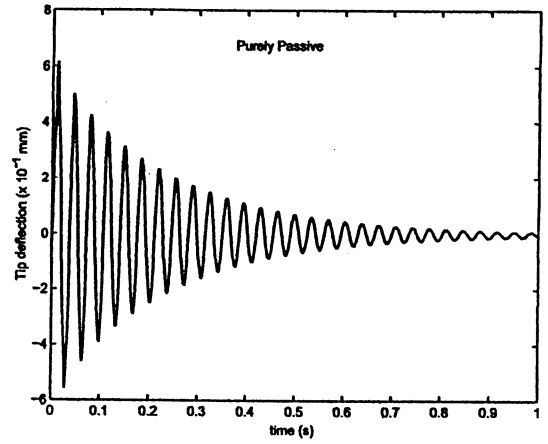

(a) Uncontrolled tip deflection

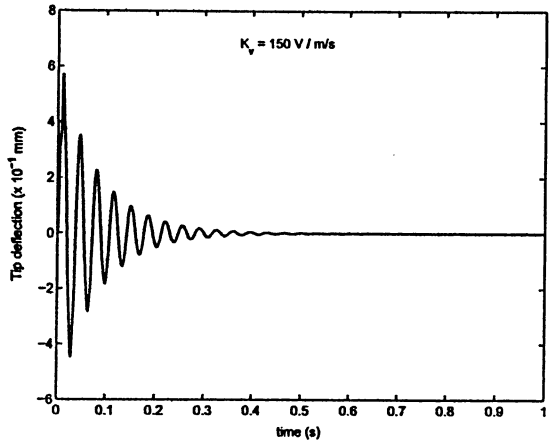

(b) Controlled tip deflection

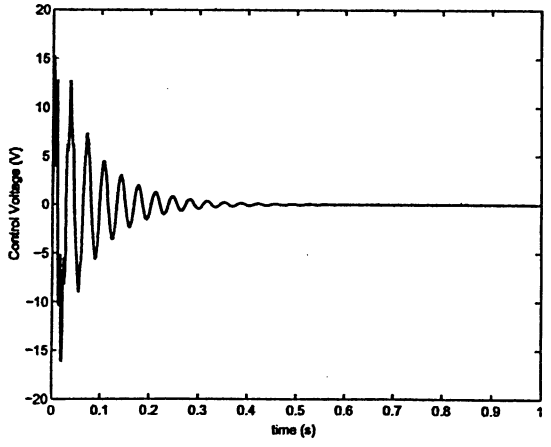

(c) Actuator voltage

Figure 4.11: Tip deflection and actuator voltage of a fully constrained layer beam subjected to a triangular impulse load at the free end.

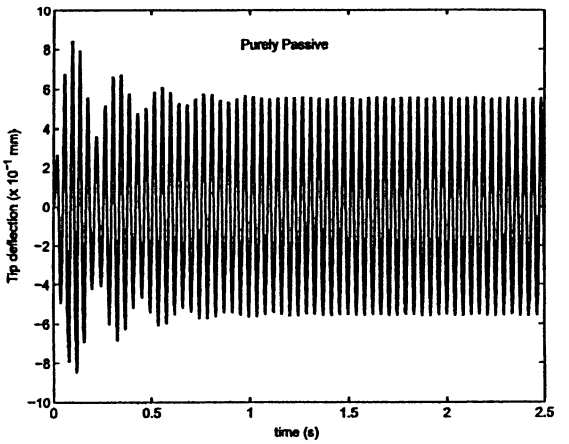

(a) Uncontrolled tip deflection

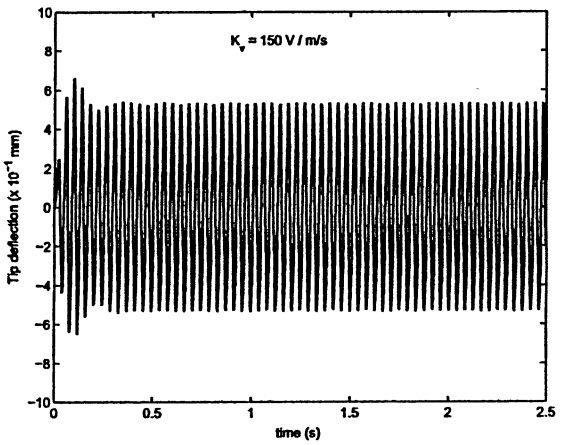

(b) Controlled tip deflection

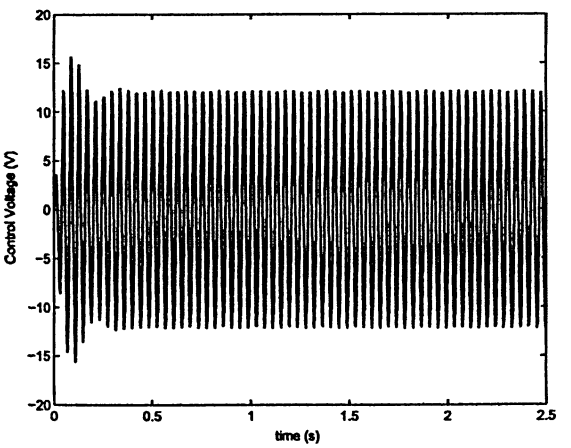

(c) Actuator voltage

Figure 4.12: Tip deflection and actuator voltage of a fully constrained layer beam subjected to a harmonic force $(0.1sin150t)$ at the free end.

the breakdown range of about $200\,V$ for most piezoelectric polymers.

4.2.2 Case of partially-constrained-layer beam

Unlike the scenario described in the preceding section, the system of interest here involves a host beam whose span is partially covered with the viscoelastic layer and piezoelectric layer as schematically depicted in Fig. 4.13. The beam is meshed with six finite elements along the

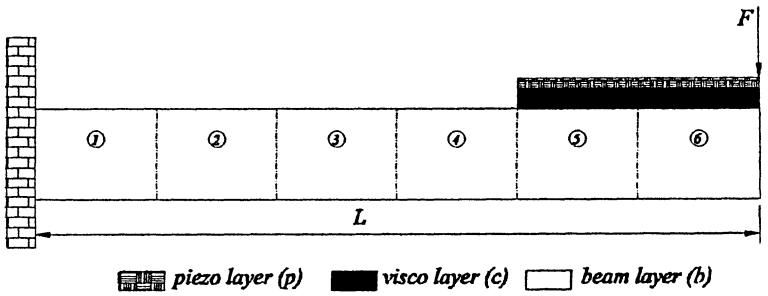

Figure 4.13: Schematic of a partially-constrained-layer beam

span. The first two elements from the free end are covered with the constrain layer. The gain $K_v = 1500\,Vs\,/\,m$. While any gain is theoretically selectable provided its use does not induce instability in the system, it is instructive that the gains are selected so as to yield actuating voltages that are not in the breakdown voltage range of the piezoelectric material.

The results obtained by applying a triangular impulse force and an harmonic load are depicted in Figs. 4.14 and 4.15, respectively. Figs. 4.14(a) and 4.15(a) indicate that the sole use of passive damping of the viscoelastic layer has negligible effect. The beat phenomenon in the latter is a reflection of the propinquity of the forcing frequency of the harmonic load and the second natural frequency of the system.

Again as observed in the case of fully-constrained-layer beam, active-passive damping, as demonstrated by Figs. 4.14(b) and 4.15(b), is superior to passive damping.

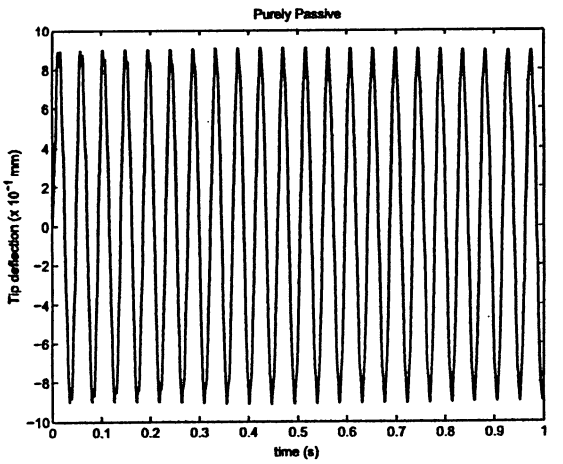

(a) Uncontrolled tip deflection

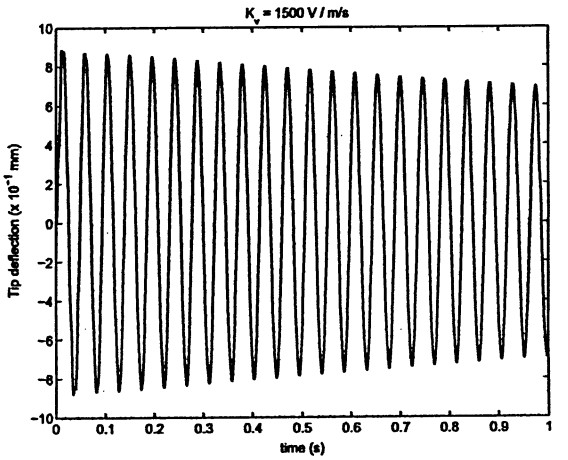

(b) Controlled tip deflection

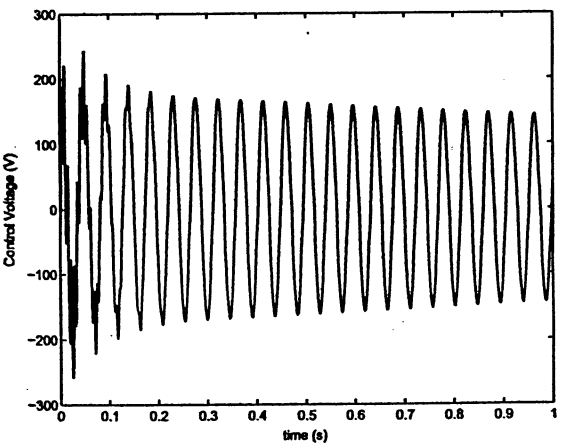

(c) Actuator voltage

Figure 4.14: Tip deflection and actuator voltage of a partially-constrained-layer beam subjected to a triangular impulse load at the free end.

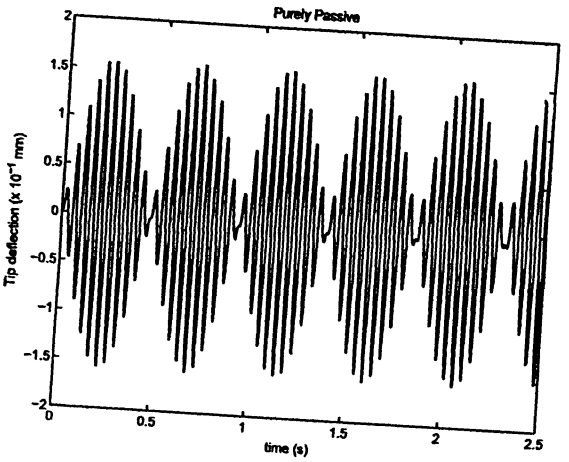

(a) Uncontrolled tip deflection

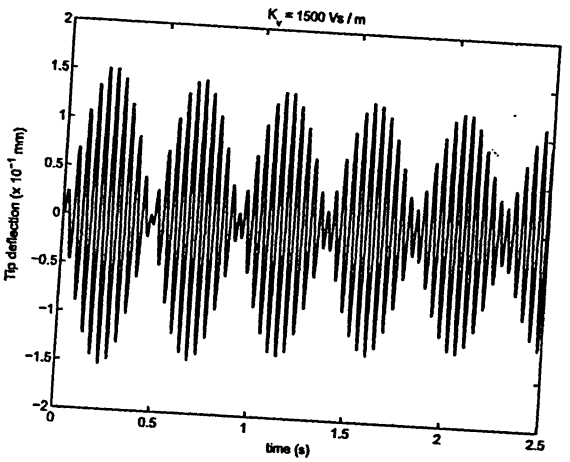

(b) Controlled tip deflection

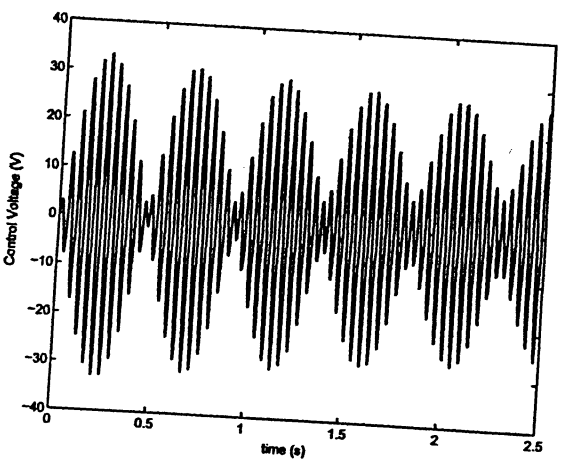

(c) Actuator voltage

Figure 4.15: Tip deflection and actuator voltage of a partially-constrained-layer beam subjected to a harmonic force $(0.1sin150t)$ at the free end.

Chapter 5

Conclusion

A quasi-two-dimensional finite element formulation has been presented for the analysis of active-passive constrained layer beams. The field variables are interpolated through the thickness via the use of polynomials and are interpolated along the span by using cubic Lagrange finite elements. The major inferences from the study include:

1. The formulation is effective for sandwich beams.
2. In the typical three-layer sandwich beam scenario (i.e., all layers are made from elastic material), the formulation is invariant to the relative stiffness between the middle (or core) layer and the outer layers.
3. The formulation avoids the anti-plane assumption that is common in other higher-order formulations.
4. The formulation allows the simulation of more boundary constraints. Specifically, it is possible to constrain each layer independent of the others.
5. The formulation does not require many degrees of freedom or elements to yield highly accurate results, where the benchmark are the traditional two-dimensional formulation using commercial software NASTRAN and ABAQUS.

Having stated the above, there are areas for further investigation. These include, for example:

1. The extension to nonlinear scenarios, geometric and/or and material nonlinearity.
2. The extension of the concept to viscoelastic plates and shells.
3. The use of different viscoelastic constitutive relations and different solution methods.

References

[1] R. Stanway, J. A. Rongong and N. D. Sims, *Active Constrained-Layer Damping: a State-of-the-Art Review*. Journal of Systems and Control Engineering, **217**, 437-456, 2003.

[2] X. Q. Peng, K. Y. Lam and G. R. Liu, *Active Vibration Control of Composite Beams with Piezoelectrics: A FEM model with Third Order Theory*. Journal of Sound and Vibration, **209**, 635-650, 1998.

[3] S. Yi, S. F. Ling and M. Ying, *Finite Element Analysis of Composite Structures With Smart Constrained Layer Damping*. Elsevier Science, **29**, 265-271, 1998.

[4] V. Balamurugan and S. Narayanan, *Finite Element Formulation and Active Vibration Control Study on Beams Using Smart Constrained Layer Damping (SCLD) Treatment*. Journal of Sound and Vibration, **2**, 227-250, 2002.

[5] D.F. Golla and P.C. Hughes, *Dynamics of viscoelastic - a time domain, Finite Element Formulation*. Journal of Applied Mechanics, **52**, 897-906, 1985.

[6] D.J. McTavish and P.C. Hughes, *Modeling of Linear Viscoelastic Space Structures*. Journal of Vibration and Acoustics, **115**, 103-110, 1993.

[7] J. X. Gao and W. H. Liao, *Vibration Analysis of Simply Supported Beams with Enhanced Self-Sensing Active Constrained Layer Damping Treatments*. Elsevier Science, **280**, 329-357, 2005.

[8] Y. Shi, H. Hua and H. Sol, *The Finite Element Analysis and Experimental Study of Beams with Active Constrained Layer Damping Treatments*. Journal of Sound and Vibration, **278**, 343-363, 2004.

[9] D. Sun and L. Tong, *A Compressional-Shear model for Vibration Control of Beams with Active Constrained Layer Damping*. Elsevier Science, **46**, 1307-1325, 2004.

[10] K. H. Ha, *Finite Element Analysis of Sandwich Plates: an Overview*. Computers and Structures, **37**, 397-403, 1990.

[11] S. Oskooei and J. S. Hansen, *Higher-Order Finite Element for Sandwich Plates*. AIAA Journal, **38**, 525-533, 2000.

[12] A. Nabarrete, S. Frascino, M. de Almeida and J. S. Hansen, *Sandwich-Plates Vibration Analysis: Three-Layer Quasi-Three-Dimensional Finite Element Model*. AIAA Journal, **41**, 1547-1555, 2003.

[13] P. K. Mallick, *Composites Engineering Handbook*. Marcel Dekker Inc. New York, 1997.

[14] M. A. Bhatti, *Advanced Topics in Finite Element Analysis of Structures*. John Wiley & Sons, New Jersey, 2006.

[15] A. P. Boresi and R. J. Schmidt, *Advanced Mechanics of Materials*. John Wiley & Sons, New Jersey, Sixth Edition, August 2003.

[16] X. D. Zhang and C. T. Sun, *Formulation of an Adaptive Sandwich Beam*. Journal of Smart Materials and Structures, **5**, 814-823, 1996.

[17] M. W. Hyer, *Stress Analysis of Fiber-Reinforced Composite Materials*. McGraw-Hill, 1998.

[18] A. C. Galucio, J. F. De and R. Ohayon, *A Fractional Derivative Viscoelastic Model for Hybrid Active-Passive Damping Treatments in Time Domaine-Applications to sandwich Beams*. Journal of Intelligent Material Systems and Structures, **16**, 33-47, 2005.

[19] A. C. Galucio, J. F. De and R. Ohayon, *Finite Element Formulation of Viscoelastic Sandwich Beams using Fractional Derivative Operators*. Journal of Computational Mechanics, **33**, 282-291, 2003.

[20] F. B. Hildebrand, *Methods of Applied Mathematics*. Dover Publications Inc. New York, Second Edition, 1965.

[21] D. L. Logan, *A First Course in the Finite Element Method*. Brooks & Cole Third Edition, 2002.

[22] O. C. Zienkiewicz and R.L. Taylor, *FEM for Solid and Structural Mechanics*. Elsevier Butterworth-Heinemann, Burlington, 2005.

[23] K. J. Bathe and E. L. Wilson, *Numerical Methods in Finite Element Analysis*. Prentice-Hall, New Jersey, 1976.

[24] V. S. Sokolinsky and S. R. Nutt, *Consistent Higher-Order Dynamic Equations for Soft-Core Sandwich Beams*. AIAA Journal, **42**, 374-382, 2004.

[25] V. S. Sokolinsky, H. F. Von Bremen, J. A. Lavoie and S. R. Nutt, *Analytical and Experiemental Study of Free Vibration Response of Soft-Core Sandwich Beams*. Journal of Sandwich Structures and Materials, **6**, 239-261, May 2004.